FZD-487

Turbulent Dispersion of Bubbles in Poly-dispersed Gas-Liquid Flows in a Vertical Pipe

and

Validation of the Multiple Velocity Multiple Size Group (CFX10.0 N x M MUSIG) Model for Polydispersed Multiphase Flows

Jun-Mei Shi, Ulrich Rohde, Horst-Michael Prasser

September 2007

Wissenschaftlich-Technische Berichte
FZD-487 2007 · ISSN 1437-322X

WISSENSCHAFTLICH-TECHNISCHE BERICHTE

Forschungszentrum Dresden Rossendorf

Wissenschaftlich-Technische Berichte
FZD-487
September 2007

Jun-Mei Shi, Ulrich Rohde, Horst-Michael Prasser

Validation of the Multiple Velocity Multiple Size Group (CFX10.0 N x M MUSIG) Model for Poly-dispersed Multiphase Flows

Technical Report

Forschungszentrum Dresden Rossendorf

Technischer Sachbericht
Validierung des N x M MUSIG Modells für polydisperse Mehrphasenströmungen

Technical Report
Validation of the Multiple Velocity Multiple Size Group (CFX10.0 N x M MUSIG) Model for Poly-dispersed Multiphase Flows

Reaktorsicherheitsforschung-Vorhaben-Nr./ Reactor Safety Research-project No.: 150 1265

Vorhabenstitel: **Aufbau und Durchführung von Experimenten an der Mehrzweck-Thermohydraulikversuchsanlage TOPFLOW für generische Untersuchungen von Zweiphasenströmungen und die Weiterentwicklung und Validierung von CFD-Codes.**

Project Title: **Construction and execution of experiments at the multi-purpose thermal hydraulic test facility TOPFLOW for generic investigations of two-phase flows and the development and validation of CFD codes.**

Autoren / Author(s): **Jun-Mei Shi, Ulrich Rohde, Horst-Michael Prasser**

Dienststelle der Autoren / Performing Organisation: **Forschungszentrum Dresden-Rossendorf e.V. Institut für Sicherheitsforschung**

Berichtsdatum / Publication Date: **September 2007**

Berichts-Nr. / Report-No.: **FZD-487**

Das diesem Bericht zugrunde liegende Vorhaben wurde mit Mitteln des Bundesministeriums für Wirtschaft und Technologie unter dem Förderkennzeichen 150 1265 gefördert. Die Verantwortung für den Inhalt dieser Veröffentlichung liegt bei den Autoren.

Berichtsblatt

1. ISBN oder ISSN	2. Berichtsart Technischer Fachbericht
3a. Titel des Berichts Validierung des N x M MUSIG Modells für polydisperse Mehrphasenströmungen	
3b. Titel der Publikation	
4a. Autoren des Berichts (Name, Vorname(n)) Jun-Mei Shi, Ulrich Rohde, Horst-Michael Prasser	5. Abschlussdatum des Vorhabens 30.09.2006
	6. Veröffentlichungsdatum September 2007
4b. Autoren der Publikation (Name, Vorname(n))	7. Form der Publikation Broschüre
8. Durchführende Institution(en) (Name, Adresse) Forschungszentrum Dresden-Rossendorf e.V. Institut für Sicherheitsforschung Postfach 510119 01314 Dresden	9. Ber.Nr. Durchführende Institution
	10. Förderkennzeichen *) 150 1265
	11a. Seitenzahl Bericht
	11b. Seitenzahl Publikation
13. Fördernde Institution (Name, Adresse) Bundesministeriums für Wirtschaft und Technologie (BMWi) 11019 Berlin	12. Literaturangaben 19
	14. Tabellen 4
	15. Abbildungen 17
16. Zusätzliche Angaben	
17. Vorgelegt bei (Titel, Ort, Datum)	

18. Kurzreferat

Zur Simulation disperser Zweiphasenströmungen werden CFD Codes zur Berechnung der lokalen Partikeldichte und ihrer Größenverteilung benötigt. Diese Größen beeinflussen sowohl die Vermischung, die Reaktionsraten im Fall heterogener chemischer Reaktionen oder den Massen- und Energietransfer zwischen den Phasen als auch die Dynamik der Strömung. Für diesen Zweck wurde ein Mehrblasenklassenmodell (MUSIG) entwickelt. Es ist in den CFD Codes CFX-4 und CFX-5 verfügbar. Das Modell basiert auf einer Populationsbilanz und einem Zwei-Fluid-Ansatz. Die disperse Phase wird dabei in N Gruppen unterteilt. Zur Begrenzung des Rechenaufwands wird nur ein Geschwindigkeitsfeld für alle Blasenklassen berücksichtigt. Dieses Modell gestattet die Berücksichtigung einer genügend großen Anzahl von Blasenklassen für Blasenkoaleszenz und –zerfall. Allerdings ist die Anwendung dieses Ansatzes auf homogene Strömungen begrenzt und wird daher als homogenes MUSIG-Modell bezeichnet. Es versagt, wenn eine heterogene Partikelbewegung simuliert werden soll. In vielen Strömungen sind die s.g. Non-Drag-Kräfte für die Partikelbewegung von Bedeutung. Insbesondere hat die Lift-Kraft im Fall großer, deformierbarer Blasen, die durch Asymmetrien der Nachlaufströmung einer Blase bestimmt wird das entgegengesetzte Vorzeichen der scherinduzierten Lift-Kraft bei kleinen Blasen. Die Separation der kleinen und großen Blasen kann mit dem homogenen MUSIG-Modell nicht simuliert werden. Um diese Beschränkung zu überwinden wurde in Zusammenarbeit mit dem Codeentwickler ANSYS ein effizientes inhomogenes MUSIG-Modell entwickelt. Dieses neue Modell mit mehreren Geschwindigkeitsgruppen für die disperse Phase beruht auf einem Multi-Fluid-Ansatz unter Einbeziehung einer Populationsbilanz. Im vorliegenden Bericht wird die Validierung des Modells diskutiert.

19. Schlagwörter Blasenströmung, Impulsaustausch, Blasenkräfte, Mehrblasenklassenmodell	
20. Verlag	21. Preis

Document Control Sheet

1. ISBN or ISSN	2. Type of Report Technical Report
3a. Report Title Validation of the Multiple Velocity Multiple Size Group (CFX10.0 N x M MUSIG) Model for Poly-dispersed Multiphase Flows	
3b. Title of Publication	
4a. Author(s) of the Report (Family Name, First Name(s)) Jun-Mei Shi, Ulrich Rohde, Horst-Michael Prasser	5. End of Project 30.09.2006
	6. Publication Date September 2007
4b. Author(s) of the Publication (Family Name, First Name(s))	7. Form of Publication Booklet
8. Performing Organisation(s) (Name, Address) Forschungszentrum Dresden-Rossendorf e.V. Institut für Sicherheitsforschung Postfach 510119 01314 Dresden	9. Originator's Report No.
	10. Reference No.*) 150 1265
	11a. No. of Pages Report
	11b. No. of Pages Publication
13. Sponsoring Agency (Name, Address) Bundesministeriums für Wirtschaft und Technologie (BMWi) 11019 Berlin	12. No. of References 19
	14. No. of Tables 4
	15. No. of Figures 17
16. Supplementary Notes	
17. Presented at (Title, Place, Date)	

18. Abstract

To simulate dispersed two-phase flows CFD tools for predicting the local particle number density and the size distribution are required. These quantities do not only have a significant effect on rates of mixing, heterogeneous chemical reaction rates or interfacial heat and mass transfers, but also a direct relevance to the hydrodynamics of the total system, such as the flow pattern and flow regime. The Multiple Size Group (MUSIG) model available in the commercial codes CFX-4 and CFX-5 was developed for this purpose. Mathematically, this model is based on the population balance method and the two-fluid modeling approach. The dispersed phase is divided into N size classes. In order to reduce the computational cost, all size groups are assumed to share the same velocity field. This model allows to use a sufficient number of particle size groups required for the coalescence and breakup calculation. Nevertheless, the assumption also restricts its applicability to homogeneous dispersed flows. We refer to the CFX MUSIG model mentioned above as the homogeneous model, which fails to predict the correct phase distribution when heterogeneous particle motion becomes important. In many flows the non-drag forces play an essential role with respect to the bubble motion. Especially, the lift force acting on large deformed bubbles, which is dominated by the asymmetrical wake, has a direction opposite to the shear induced lift force on a small bubble. This bubble separation cannot be predicted by the homogeneous MUSIG model. In order to overcome this shortcoming we developed an efficient inhomogeneous MUSIG model in cooperation with ANSYS CFX. A novel multiple velocity multiple size group model, which incorporates the population balance equation into the multi-fluid modeling framework, was proposed. The validation of this new model is discussed in this report.

19. Keywords

Bubbly flow, momentum transfer, bubble forces, multi bubble size group modelling

20. Publisher	21. Price

This report is part of a series, which comprise following reports:

- Construction and execution of experiments at the multi-purpose thermal hydraulic test facility TOPFLOW for generic investigations of two-phase flows and the development and validation of CFD codes (Final project report), FZD-481,
- Experiments on upwards gas-liquid flow in vertical pipes, FZD-482,
- Experiments on two-phase flow in a vertical tube with a moveable obstacle, FZD-483,
- Experimental investigation of stratified air/water flows in a horizontal channel, FZD-484,
- Experimental investigation and CFD simulation of slug flow in horizontal channels, FZD-485,
- CFD models for polydispersed bubbly flows, FZD-486,
- Turbulent Dispersion of Bubbles in Poly-dispersed Gas-Liquid Flows in a Vertical Pipe, FZD-487,
- Validation of the Multiple Velocity Multiple Size Group (CFX10.0 N x M MUSIG) Model for Poly-dispersed Multiphase Flows, FZD-487.

All these reports are published as reports of the Forschungszentrum Dresden-Rossendorf.

Dieser Bericht ist Teil einer Serie, die folgende Einzelberichte umfasst:

- Aufbau und Durchführung von Experimenten an der Mehrzweck-Thermohydraulikversuchsanlage TOPFLOW für generische Untersuchungen von Zweiphasenströmungen und die Weiterentwicklung und Validierung von CFD-Codes (Abschlussbericht), FZD-480,
- Experimente zu aufwärtsgerichteten Gas-Flüssig Strömungen in vertikalen Rohren, FZD-482,
- Experimente zur Zweiphasenströmung in einem vertikalen Rohr mit verschiebbarem Hindernis, FZD-483,
- Experimentelle Untersuchung von geschichteten Luft/Wasser Strömungen in einem horizontalen Kanal, FZD-484,
- Experimentelle Untersuchung und CFD-Simulation von Schwallströmung in horizontalen Kanälen, FZD-485,
- CFD Modelle für polydisperse Blasenströmungen, FZD-486,
- Turbulente Blasendispersion in einer polydispersen Rohrströmung, FZD-487,
- Validierung des N x M MUSIG Modells für polydisperse Mehrphasen-strömungen, FZD-487.

Alle Berichte sind als Berichte des Forschungszentrums Dresden-Rossendorf veröffentlicht.

Contents

1 Introduction

Poly-dispersed multiphase flows are widely encountered in engineering and industrial facilities. These flows can have a complex nature, involving several flow regimes, multiple diverse particle morphologies, heterogeneous particle motions with various time scales related to a variety of particle sizes, and accompanied by particle allegation and breakage processes or even by flow regime transition. Design of these facilities and development of optimal processing techniques require a CFD tool for predicting the distribution of the particle concentration, the local particle number density and the size distribution. These quantities not only have a significant effect on the rate of mixing, reaction and the interfacial heat and mass transfer, but also a direct relevance to the hydrodynamics of the total system, such as the flow pattern and flow regime. The Multiple Size Group (MUSIG) model (Lo, 1996) available in the commercial codes CFX-4 and CFX-5 was developed for this purpose. Mathematically, this model is based on the population balance method and the two-fluid modeling approach. The dispersed phase is divided into N size classes. The population balance equation is applied to describe the mass conservation of the size classes taking into account of the inter-class mass transfer resulting from particle coalescence and breakup. In order to reduce the computational cost, all size groups are assumed to share the same velocity field. That means, one needs only to solve a set momentum equations for the entire dispersed phase. This model allows to use a sufficient number of particle size groups required for the coalescence and breakup calculation and has found a number of successful applications to large-scale industrial multiphase flow problems. Nevertheless, the assumption also restricts its applicability to homogeneous dispersed flows—the slip velocity of particles are approximately independent of particle size; and the particle relaxation time is sufficiently small relative to inertial time scales so that the asymptotic slip velocity may be considered to be attained almost instantaneously—.

We refer to the CFX MUSIG model mentioned above as the homogeneous model, which fails to predict the correct phase distribution when heterogeneous particle motion becomes important. One example is the bubbly flow in vertical pipes where the non-drag forces play an essential role on the bubble motion. Especially, the lift force acting on large deformed bubbles, which is dominated by the asymmetrical wake[1], has a direction opposite to the shear induced lift force on a small bubble. For this reason, large bubbles tend to move to the pipe core region resulting in a core void maximum whereas a wall void peak is measured for small bubbles (Lucas et al., 2003; Prasser et al., 2002). Nevertheless, this bubble separation cannot be predicted by the homogeneous MUSIG model as reported in (Krepper and Prasser, 2000).

In order to overcome this shortcoming we developed an efficient inhomogeneous MUSIG model in cooperation with ANSYS CFX. A novel multiple velocity multiple size group model, which incorporates the population balance equation into the multi-fluid modeling framework, was proposed (Krepper et al., 2003). The original concept was to model bubbles with opposite lift force separately by using two velocity groups and allow each velocity group to have a further size discretization. In this way, the inhomogeneous motion of the dispersed phase is dealt with in an efficient way along the line of the

[1] For air bubbles in pure water, the lift force due to the asymmetrical wake becomes dominating over the shear induced mechanism at a critical value of the Eötvös number 10.7, corresponding to a bubble diameter about 5.8 mm under the atmosphere pressure and room temperature (Tomyiama, 1998; Tomyiama et al., 1995).

MUSIG model. This concept was adopted by the CFD code provider ANSYS CFX and has led to a general framework covering all possible class model variants (Zwart et al., 2003), namely dividing the dispersed phase into N fields (dispersed fluids), each allowing an arbitrary number of sub-size classes (e.g., M_i). We refer to it as the $N \times M$ MUSIG model. Based on a preliminary investigation using the $N \times 1$ variant, namely N velocity groups and each has one size groups (Shi et al., 2004a,b), this model has been implemented and released as a beta package of CFX10.0. In the folowing text we provide a brief description of the model concept and a detailed model evaluation based on the numerical simulation of gas-liquid flows in a vertical pipe with an inner diameter $D = 195.3$mm, a test section of the TOPFLOW facility at FZR (Prasser et al, 2003) and the corresponding experimental data.

2 The $N \times M$ MUSIG model

Using the multi-fluid modeling approach we might model the dispersed phase by N fields (separated phases) according to the particle sizes to account for the inhomogeneity in the dispersed phase flow. Hence N velocity fields are to be solved for the dispersed phase. For this reason, we refer to these fields as velocity groups. We further divide each velocity group into a sub-division of size cuts (e.g., M_i) and assume that they share the same velocity field corresponding to this velocity group as in the homogeneous MUSIG model. Then only a continuity equation based on the population balance method has to be solved for the mass conservation of a sub-size class coupled with the coalescence and breakup processes. Without loss of the generality, the model equations are presented for an isothermal, laminar multiphase flow of Newtonian fluids and without mass transfer between the continuous and the dispersed phase.

The governing equations describing the mass and momentum conservation for the continuous phase are as follows:

$$\frac{\partial}{\partial t}(r_\ell \rho_\ell) + \nabla \cdot (r_\ell \rho_\ell \mathbf{U}_\ell) = 0 \tag{1}$$

$$\frac{\partial}{\partial t}(r_\ell\, \rho_\ell \mathbf{U}_\ell) + \nabla \cdot (r_\ell\, \rho_\ell \mathbf{U}_\ell \mathbf{U}_\ell) = -r_\ell\, \nabla p - \nabla \cdot (r_\ell\, \underline{\underline{\tau_\ell}}) + r_\ell\, \rho_\ell \mathbf{g} + \mathbf{F}_\ell + \mathbf{I}_\ell \tag{2}$$

where r_ℓ is the volume fraction of the continuous phase, $\mathbf{F}_\ell$ the body force excluding the gravity and $\mathbf{I}_\ell$ the momentum interaction between the continuous and dispersed phase. $\underline{\underline{\tau_\ell}}$ is the stress tensor defined as

$$\underline{\underline{\tau_\ell}} = -\mu_\ell \left(\nabla \mathbf{U}_\ell + \nabla^{\mathbf{T}} \mathbf{U}_\ell) - \frac{1}{3} (\nabla \cdot \mathbf{U}_\ell)\, \underline{\underline{\mathbf{I}}} \right) \tag{3}$$

Defining r_m to be the volume fraction of the velocity group m of the dispersed phase, its continuity equation can be written as

$$\frac{\partial}{\partial t}(\rho_m\, r_m) + \nabla \cdot (\rho_m\, r_m \mathbf{U_m}) = S_m \tag{4}$$

where S_m is the mass source term, to be specified in eq. (8). The momentum equation can be expressed as

$$\frac{\partial}{\partial t}(\rho_m\, r_m \mathbf{U_m}) + \nabla\cdot(\rho_m\, r_m \mathbf{U_m}\mathbf{U_m}) = -\, r_m \nabla p - \nabla\cdot(r_m\, \underline{\underline{\tau_{\mathbf{m}}}}) + r_m \rho_m \mathbf{g} + \mathbf{F_m} + \mathbf{I}_{\ell,\mathbf{m}} + \mathbf{I}_{\mathbf{d},\mathbf{m}} \tag{5}$$

where $\mathbf{I}_{\ell,\mathbf{m}}$ represents the interaction with the continuous phase (e.g., the interfacial forces). The quantity $\mathbf{I}_{\mathbf{d},\mathbf{m}}$ is introduced to denote the secondary momentum transfer, which is related to the mass transfer between the velocity groups resulting from particle coalescence and breakup. Specification of this term is described in detail in (Krepper et al., 2003). For simplicity the same pressure field as the continuous phase is assumed above.

The population balance equation is applied to each sub-size group. Assume that the size group i is a sub-division of the velocity group m. Defining r_d and r_i to be the volume fraction of the total dispersed phase and of the size group i, respectively, and f_i and $f_{m,i}$ to be respectively the size fraction of the size group i in the total dispersed phase and in the velocity group m, the different flavors of size fractions are related by

$$r_i = r_d\, f_i = r_m\, f_{m,i} \tag{6}$$

With these definitions, and recognizing that velocity fields are homogeneous for all size groups within a velocity group m, the population balance equation for the size group i leads to

$$\frac{\partial}{\partial t}\left(\rho_m\, r_m\, f_{m,i}\right) + \nabla\cdot\left(\rho_m\, r_m\, \mathbf{U}_m\, f_{m,i}\right) = S_{m,i} \tag{7}$$

where $S_{m,i}$ is the mass source term.

Then the mass source S_m in eq. (4) can be specified, i.e.

$$S_m = \sum_{i=1}^{N_m} S_{m,i} \tag{8}$$

where N_m is the number of the sub-divisions in the velocity group m, and obviously, we have $\sum_m S_m = 0$.

In the case that coalescence and breakup are the only mass transfer mechanism, $S_{m,i}$ can be expressed as follows

$$S_{m,i} = B_{i,B} - D_{i,B} + B_{i,C} - D_{i,C} \tag{9}$$

where $B_{i,B}$ and $D_{i,B}$ are respectively the birth and death rate of the size group i due to breakup and $B_{i,C}$ and $D_{i,C}$ are the coalescence-related counterparts. They are defined as follows

$$B_{i,B} = \rho_d\, r_d \sum_{j>i} B_{ji}\, f_j, \tag{10}$$

$$D_{i,B} = \rho_d\, r_d\, f_i \sum_{k<i} B_{ik}, \tag{11}$$

$$B_{i,C} = (\rho_d\, r_d)^2\, \frac{1}{2} \sum_{j\le i} \sum_{k\le i} C_{jk}\, f_j\, f_k \frac{m_j + m_k}{m_j\, m_k}\, X_{jk\to i}, \tag{12}$$

$$D_{i,C} = (\rho_d\, r_d)^2 \sum_{j} C_{ij}\, f_i\, f_j\, \frac{1}{m_j} \tag{13}$$

where B_{ji} is the specific breakup rate from size group j to i, C_{jk} is the specific coalescence rate between size group j and k, m_i represents the mass of a single particle of the group i. $X_{jk\to i}$ is a factor projecting the corresponding part of the birth particle into the ith size group, defined as follows

$$X_{jk\to i} = \begin{cases} \frac{(m_j+m_k)-m_{i-1}}{m_i-m_{i-1}} & \text{if} \quad m_{i-1} < m_j + m_k \leq m_i \\ \frac{m_{i+1}-(m_j+m_k)}{m_{i+1}-m_i} & \text{if} \quad m_i < m_j + m_k < m_{i+1} \\ 1 & \text{if} \quad m_j + m_k \geq m_{max} = m_i \\ 0 & \text{else} \end{cases} \tag{14}$$

with $\sum_i X_{jk\to i} = 1$. In addition, the sum of the net mass source over all size groups should vanish, i.e. $\sum_i (B_{i,B} - D_{i,B}) = 0$ and $\sum_i (B_{i,C} - D_{i,C}) = 0$.

3 Model evaluation

Extensive experiments were carried out for gas-liquid flows in a vertical pipe with a inner diameter of 195.3 mm on the TOPFLOW facility at Forschungszentrum Rossendorf. The radial distributions of the gas volume fraction, the gas velocity and the bubble size fraction at various distance from the gas injection plane were obtained. The test facility and experiment are described in section 3.1. These experimental data are very useful for the validation of the interfacial force models and models for the coalescence and breakup process. In order to evaluate the performance of the $N \times M$ MUSIG model, we applied this model to simulate the flow evolution in the test section of the TOPFLOW facility. The numerical results were compared with the corresponding measurement data.

3.1 Experimental facility

The test section is equipped with a so-called "variable gas injection system" is schematically illustrated by using Fig. 3.1. The gas can be injected from six units. Each unit has three annular distributing chambers, from which gas or steam enters the test section via a number of orifices in the pipe wall (see Fig. 3.2). Two different injection diameters allow to change the primary bubble size and to study its influence on the flow structure. In particular, the upper and the lower chambers have 72 orifices of 1 mm diameter, the central chamber has 32 orifices of 4 mm. The orifices are uniformlly distributed along the circumference of the sparger in order to ensure the flow to be axi-symmetrical in the vertical pipe. With this construction the gas can be injected at various heights with the indices from A to R.

Two wire-mesh sensors, consiting of 64 receiver and 64 transmitter wires, are mounted close to the upper end of the vertical pipe to measure the local instantaneous gas volume fraction. The grid resolution is 3mm and the sampling frequency is 2500Hz. From this data, cross-section averaged gas fractions as well as radial gas fraction profiles can be calculated. The radial gas velocity profile at the sensor location was obtained by means of a point-to-point cross-correlation between the signals of both

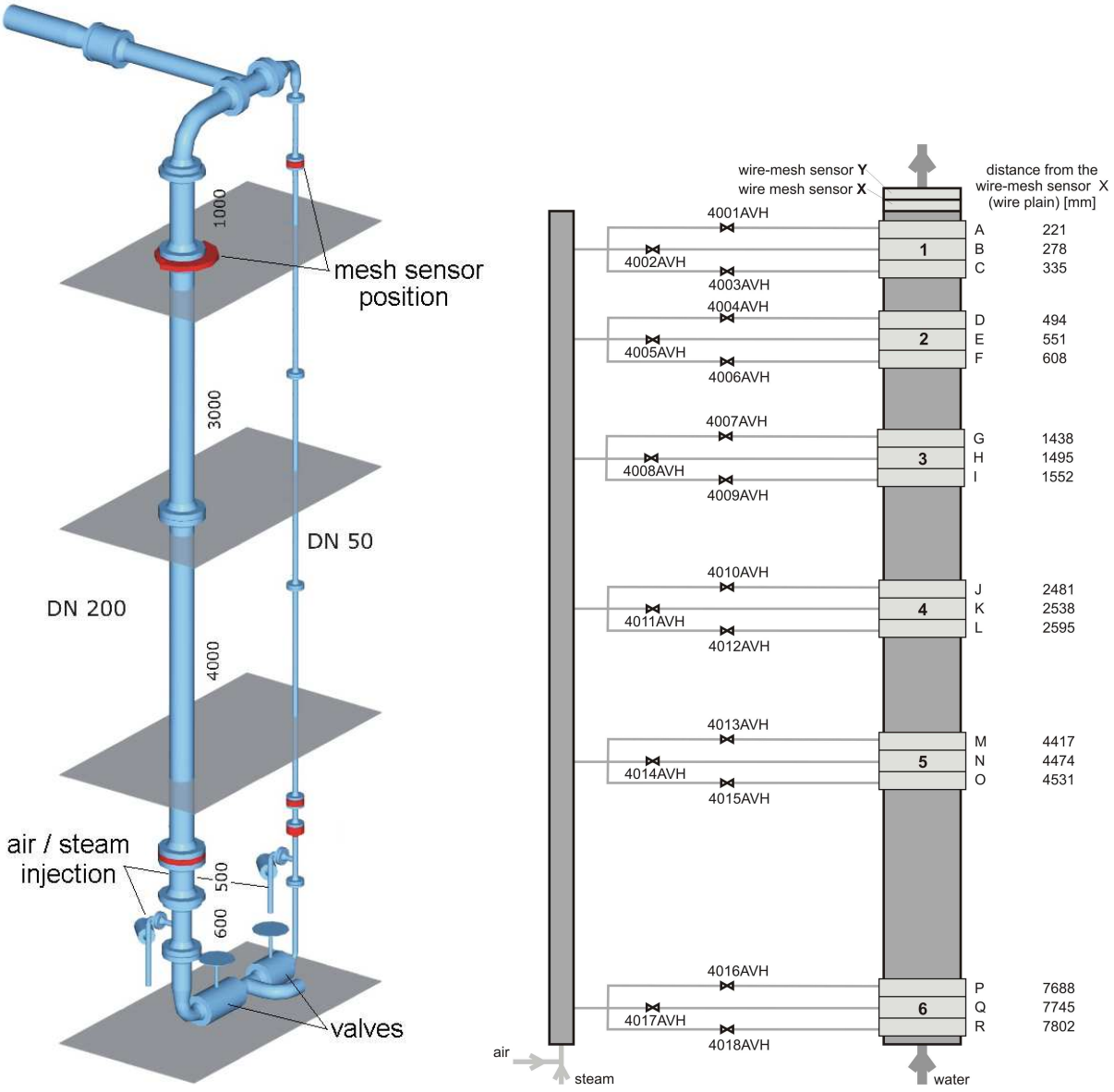

Fig. 3.1: A scheme of the test section.

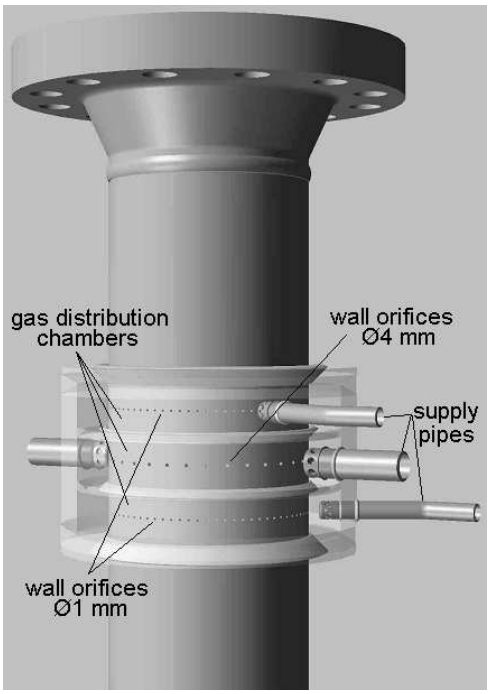

Fig. 3.2: A scheme of the gas injection chamber

sensors placed in a distance of 63 mm from each other. The high resolution and frequency of the mesh sensors allow identifying individual bubbles. Hence the bubble size distribution can be obtained.

3.2 Test cases and numerical settings

In the experiments, the superficial velocities ranged from 0.04 to 8 m/s for the gas phase and from 0.04 to 1.6 m/s for the liquid. In this way, the experiments cover the range from bubbly to churn turbulent flow regimes. Two test cases, one with low gas concentration (074) and the other with high gas concentration (107) were selected for the model evaluation. In the case 074, the liquid and the gas phase have a superficial velocity $U_{\ell,sup} = 1.017$ m/s and and $U_{g,sup} = 0.0368$ m/s, respectively. This corresponds to an average gas concentration of about 3.5%. In comparison, the test case 107 has an average gas concentration of about 13%, estimated based on the fluid and the gas superficial velocity, $U_{\ell,sup} = 1.017$ m/s and $U_{g,sup} = 0.140$ m/s. The measurement data indicate that the local maximum gas volume fraction reaches as high as 35%. In this case, not only the coalescence and breakup model become challenged, the high volume fraction effects on the interfacial force closures aslo need to be considered. In both test case, only the experiments with 72 orifices of 1 mm diameter and under the condition of an isothermal temperature of $30\,°$C and normal pressure were considered. In addition, in order to save computational effort, the gas injection was defined at the plane R (refer to Fig. 3.1). The numerical results at the planes located at various distantances from the injection plane corresponding to the experimental case were used for comparison.

In the numerical simulation, the gas flow from each orifice was modelled as a point mass source. The bubbles were decomposed into 2 velocity groups and 21 size groups. Details are given in section 4.1 and section 5.1. The decomposition of the velocity

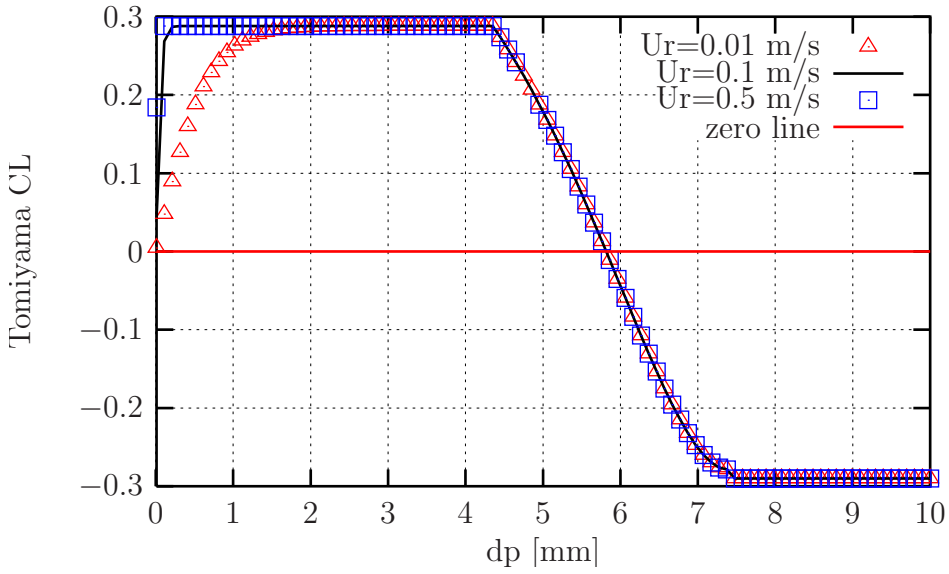

Fig. 3.3: Lift force coefficient according to the Tomiyama correlation.

groups were rough based to the sign of the lift force acting on them. According to (Tomyiama et al., 1995), the lift force on a bubble changes the sign when the Eötvös number exceeds a critical value, say about 10.7 for the current air-water system under ambient temperature and pressure, corresponding to a bubble diameter about 5.8 mm (see Fig. 3.3).

The physical model is as follows. Both the gas and the liquid phase are considered as incompressible fluids. For the turbulence modeling, the k-ω SST model was applied to the liquid phase turbulence in the present study. Particle induced turbulence was accounted for by using the enhanced eddy viscosity model by Sato et. al. (Sato and Sekoguchi, 1975; Sato et al., 1981). The dispersed phase turbulence was treated by an algebraic model assuming the kinematic eddy viscosity to be proportional to the value of the continuous phase, i.e. $\nu_{t,p} = \nu_{t,f}/\sigma_p$. The interfacial force models are: the Grace model for the drag force (Grace and Weber, 1982), the Tomiyama correlation for the lift and wall lubrication force (Tomyiama, 1998), and the FAD model for the turbulence dispersion force (Burns et al., 2004; Shi et al., 2005). The added mass force was neglected for the stationary fully developed flow considered here. The details of the non-drag force models can be found in (Shi et al., 2004c). If no explicit statement is given, a coefficient $CTD = 1.0$ was applied for FAD model. The bubble coalescence was considered by the model of Prince and Blanch (Prince and Blanch, 1990) and the breakup process was described by applying the Luo and Svendsen (Luo and Svendsen, 1996) model. Various model coefficients were applied for the calibration.

A computational domain consisting of a 60 degree sector of the pipe with the symmetry condition on both sector faces was applied in the simulation. The origin of the coordinate system is located at the injection plane R. The inlet boundary for the liquid phase is located at $hin = -4.12904$ [m]. In the first stage of the validation (section 4.2), a uniform volume fraction distribution was assumed for the liquid at the inlet together with a $1/7$-th power inlet velocity profile $U_{in} = 1.224U_0\,(1 - r^*)^{1/7}$, where U_0 is the mean velocity and $r^* = 2r/D$ the dimensionless radial coordinate. The radial velocity was assumed to be null. In addition, a medium turbulence intensity (5%) was assigned there. In order to reduce the uncertainty due to inappropriate inlet condi-

tion, all the other calculations were carried out by assigning a fully developed flow at the inlet (for the velocity and turbulence quantity profiles). The outlet was located at $hout = 8.00002$ [m], where an averaged static pressure equal to the atmospheric pressure P_0 was assigned. No-slip condition together with the CFX5 build-in wall functions for the turbulence models was applied for the liquid at the wall, whereas a free-slip wall condition was assumed for the gas. The pressure field was initialized using the expression $P = P_0 + \rho_\ell |\mathbf{g}|(hout - z)$, where z is the vertical coordinate. Further details of the numerical settings are described in section 4.1 and section 5.1.

Compared with our previous study for the non-drag force validation (Shi et al., 2004c), a much higher grid resolution, especially in the region around the gas injection plane, was applied. Considering the high grid resolution being applied, we believe that the numerical results are grid-independent.

It is worth pointing out that the bubble coalescence and breakup models are still in an inmature developing status. As a first step, we choose the widely applied models in the literature, namely the Prince and Blanch (Prince and Blanch, 1990) and the Luo and Svendson model (Luo and Svendsen, 1996), to verify the newly developed $N \times M$ MUSIG model.

4 The test case 074

4.1 Further details of the numerical settings

The gas phase was discretized into 2 velocity groups and 21 size groups as shown in Table 4.1. The bubble diameter was assumed to be in the range of 2 to 13 mm according to the measurement data and an equal-diameter discretization was applied. The gas injection from each orifice of the gas chamber was modeled as a point mass source. The bubble size distribution at the mass source points was specified based on the data measured by the X-sensor (the lower one) for the gas injected from the plane A, which is given in Tables 4.2 and 4.3. The data is normalized, namely the size fraction of each velocity group sums to one. This was required by the model implementation in a pre-released CFX code, CFX 5.8α.

The final model implementation released with CFX10.0 requires the size fraction of all bubble classes to sum to one. According to the measurement data, 0.12949% of the total injected gas belongs to the velocity group 1 and 0.87051% to the velocity group 2. Therefore, the bubble size fraction distribution at the mass source points is modified as follows

```
sfvalue1 = 0.12949*0.230726/100.0
sfvalue2 = 0.12949*0.416334/100.0
sfvalue3 = 0.12949*0.991893/100.0
sfvalue4 = 0.12949*1.2225/100.0
sfvalue5 = 0.12949*4.16243/100.0
sfvalue6 = 0.12949*10.9542/100.0
sfvalue7 = 0.12949*32.2572/100.0
sfvalue8 = 0.12949*49.7647/100.0
sfvalue9 = 0.87051*20.2955/100.0
sfvalue10 = 0.87051*19.1152/100.0
sfvalue11 = 0.87051*18.531/100.0
```

Group	Polydispersed Fluid	Diameter (mm)	Mass (kg)
Group 1	Air1	2.2619	7.1803E-09
Group 2	Air1	2.7857	1.3413E-08
Group 3	Air1	3.3095	2.2491E-08
Group 4	Air1	3.8333	3.4950E-08
Group 5	Air1	4.3571	5.1324E-08
Group 6	Air1	4.8810	7.2149E-08
Group 7	Air1	5.4048	9.7960E-08
Group 8	Air1	5.9286	1.2929E-07
Group 9	Air2	6.4524	1.6668E-07
Group 10	Air2	6.9762	2.1066E-07
Group 11	Air2	7.5000	2.6176E-07
Group 12	Air2	8.0238	3.2052E-07
Group 13	Air2	8.5476	3.8748E-07
Group 14	Air2	9.0714	4.6317E-07
Group 15	Air2	9.5952	5.4813E-07
Group 16	Air2	10.119	6.4289E-07
Group 17	Air2	10.643	7.4798E-07
Group 18	Air2	11.167	8.6395E-07
Group 19	Air2	11.690	9.9132E-07
Group 20	Air2	12.214	1.1306E-06
Group 21	Air2	12.738	1.2824E-06

Tab. 4.1: MUSIG fluid and group discretization.

sfvalue1	0.230726/100.0
sfvalue2	0.416334/100.0
sfvalue3	0.991893/100.0
sfvalue4	1.2225/100.0
sfvalue5	4.16243/100.0
sfvalue6	10.9542/100.0
sfvalue7	32.2572/100.0
sfvalue8	49.7647/100.0

Tab. 4.2: Bubble size fraction (sums to unit) distribution at the nozzle exit, velocity group 1.

sfvalue9	20.2955/100.0
sfvalue10	19.1152/100.0
sfvalue11	18.531/100.0
sfvalue12	13.4246/100.0
sfvalue13	4.8998/100.0
sfvalue14	8.05706/100.0
sfvalue15	3.24508/100.0
sfvalue16	4.87371/100.0
sfvalue17	1.94103/100.0
sfvalue18	2.52285/100.0
sfvalue19	0.806542/100.0
sfvalue20	0.701792/100.0
sfvalue21	1.58585/100.0

Tab. 4.3: Bubble size fraction (sums to unit) distribution at the nozzle exit, velocity group 2.

```
sfvalue12 = 0.87051*13.4246/100.0
sfvalue13 = 0.87051*4.8998/100.0
sfvalue14 = 0.87051*8.05706/100.0
sfvalue15 = 0.87051*3.24508/100.0
sfvalue16 = 0.87051*4.87371/100.0
sfvalue17 = 0.87051*1.94103/100.0
sfvalue18 = 0.87051*2.52285/100.0
sfvalue19 = 0.87051*0.806542/100.0
sfvalue20 = 0.87051*0.701792/100.0
sfvalue21 = 0.87051*1.58585/100.0
```

The corresponding ccl specification for the injection mass flow rates is as follows,

```
massflow1 = Air1.density*pi*rpipe*rpipe*ug leer*vofg01/vofg0
massflow2 = Air2.density*pi*rpipe*rpipe*ug leer*vofg02/vofg0
vofg01 = 0.12949 []
vofg02 = 0.87051 []
vofg0  = vofg01 + vofg02
```

The locations of the mass source points are listed below.

```
+--------------------------------------------------------------------+
 |                    User Defined Source Points                      |
 +--------------------------------------------------------------------+

 Source Point: Nozzle R12

 Domain: TopFlow
 Assigned element center (x,y,z):     8.469E-02, -4.228E-02, -2.581E-04
 User specified location (x,y,z):     8.382E-02, -4.364E-02, -3.000E-04
 Distance to user specified location:                         2.603E-06
```

```
 Source Point: Nozzle R11

 Domain: TopFlow
 Assigned element center (x,y,z):     8.459E-02,  4.221E-02, -2.581E-04
 User specified location (x,y,z):     8.382E-02,  4.364E-02, -3.000E-04
 Distance to user specified location:                         2.604E-06

 Source Point: Nozzle R10

 Domain: TopFlow
 Assigned element center (x,y,z):     8.779E-02, -3.529E-02, -2.581E-04
 User specified location (x,y,z):     8.731E-02, -3.616E-02, -3.000E-04
 Distance to user specified location:                         9.995E-07

 Source Point: Nozzle R9

 Domain: TopFlow
 Assigned element center (x,y,z):     8.772E-02,  3.524E-02, -2.581E-04
 User specified location (x,y,z):     8.731E-02,  3.616E-02, -3.000E-04
 Distance to user specified location:                         1.022E-06

 Source Point: Nozzle R8

 Domain: TopFlow
 Assigned element center (x,y,z):     9.032E-02, -2.809E-02, -2.581E-04
 User specified location (x,y,z):     9.013E-02, -2.842E-02, -3.000E-04
 Distance to user specified location:                         1.500E-07

 Source Point: Nozzle R7

 Domain: TopFlow
 Assigned element center (x,y,z):     9.029E-02,  2.805E-02, -2.581E-04
 User specified location (x,y,z):     9.013E-02,  2.842E-02, -3.000E-04
 Distance to user specified location:                         1.597E-07

Source Point: Nozzle R6

 Domain: TopFlow
 Assigned element center (x,y,z):     9.230E-02, -2.072E-02, -2.581E-04
 User specified location (x,y,z):     9.226E-02, -2.045E-02, -3.000E-04
 Distance to user specified location:                         7.665E-08

 Source Point: Nozzle R5

 Domain: TopFlow
 Assigned element center (x,y,z):     9.229E-02,  2.070E-02, -2.581E-04
 User specified location (x,y,z):     9.226E-02,  2.045E-02, -3.000E-04
```

```
Distance to user specified location:                          6.389E-08

Source Point: Nozzle R4

Domain: TopFlow
Assigned element center (x,y,z):     9.370E-02, -1.324E-02, -2.581E-04
User specified location (x,y,z):     9.369E-02, -1.233E-02, -3.000E-04
Distance to user specified location:                          8.219E-07

Source Point: Nozzle R3

Domain: TopFlow
Assigned element center (x,y,z):     9.369E-02,  1.323E-02, -2.581E-04
User specified location (x,y,z):     9.369E-02,  1.233E-02, -3.000E-04
Distance to user specified location:                          7.944E-07

Source Point: Nozzle R2

Domain: TopFlow
Assigned element center (x,y,z):     9.451E-02, -5.685E-03, -2.581E-04
User specified location (x,y,z):     9.441E-02, -4.122E-03, -3.000E-04
Distance to user specified location:                          2.456E-06

Source Point: Nozzle R1

Domain: TopFlow
Assigned element center (x,y,z):     9.450E-02,  5.677E-03, -2.581E-04
User specified location (x,y,z):     9.441E-02,  4.122E-03, -3.000E-04
Distance to user specified location:                          2.428E-06
```

As an example, some details of the computational settings of the mass source point are given below.

```
STATIC PRESSURE:
  Option = Automatic with Value
  Relative Pressure = dens*gravx*(hout-z)
END
nozloczr = -0.0003 [m]
nozradr = 0.0945 [m]
nozzlenrr = 12.0
nozalphar = 2.0*pi/72.0
nozzlemfr1 = massr1 / 6.0 / nozzlenrr
nozzlemfr2 = massr2 / 6.0 / nozzlenrr
nozdiamr = 0.0005 [m]
nozarear = 72.0*pi*nozdiamr*nozdiamr
vnozr1 = massr1/Air1.density/nozarear
vnozr2 = massr2/Air2.density/nozarear
```

```
    MUSIG FLUID: Air
      Polydispersed Fluids List = Air1,Air2
      SIZE GROUP DISTRIBUTION:
        Option = Equal Diameter
        Minimum Diameter = 2. [mm]
        Maximum Diameter = 13. [mm]
        Number of Size Groups = 21
        SIZE GROUP: Group 1
          Option = Definition
          Polydispersed Fluid = Air1
        END
        SIZE GROUP: Group 2
          Option = Definition
          Polydispersed Fluid = Air1
        END
      BREAKUP MODEL:
        Option = Luo and Svendsen
      END
      COALESCENCE MODEL:
        Option = Prince and Blanch
        Turbulence Coalescence Coefficient = 0.5
        Allow Large Group Coalescence = F
        Coalescence Mass Matrix Option = Lumped Mass
      END
  SOURCE POINT: Nozzle R1
    Option = Cartesian Coordinates
    Cartesian Coordinates = cos(0.5 *nozalphar)*nozradr, \
                            sin(0.5 *nozalphar)*nozradr, nozloczr
    FLUID: Air1
      SOURCES:
        EQUATION SOURCE: continuity
          Option = Total Fluid Mass Source
          Total Source = nozzlemfr1
          VARIABLE: vel
            Option = Cartesian Vector Components
            xValue = -1 *vnozr1*cos(0.5 *nozalphar)
            yValue = -1 *vnozr1*sin(0.5 *nozalphar)
            zValue = 0.0 [m s^-1]
          END
SOLVER CONTROL:
  ADVECTION SCHEME:
    Option = Specified Blend Factor
    Blend Factor = 1.0
  END
  CONVERGENCE CONTROL:
    Maximum Number of Iterations = 30000
    Physical Timescale = 0.0005 [s]
    Timescale Control = Physical Timescale
```

```
    END
    CONVERGENCE CRITERIA:
      Conservation Target = 0.001
      Residual Target = 1.E-4
      Residual Type = MAX
    END
    EQUATION CLASS: vf
      ADVECTION SCHEME:
        Option = Upwind
      END
    END
  END
```

A very small time step (0.0005 [s]) was applied in the above example. This was required by the preliminary model implementation in the version CFX-5.8α to ensure a good convergence. A larger time step (0.002 [s]) was used in all simulations using CFX10.0.

Considering the large amount of equations to solve, parallel calculation is necessary. An example of the partitioning information is given below.

```
Partitioning information for domain: TopFlow
```

	Elements	Vertices (Overlap)		Faces	Weight
Full mesh	194922	208169		25914	
Part. 1	25253	27916	7.5%	3169	0.125
Part. 2	25275	27968	7.5%	3211	0.125
Part. 3	23926	26499	4.4%	3857	0.125
Part. 4	26286	29007	7.6%	3170	0.125
Part. 5	25270	27787	3.6%	3922	0.125
Part. 6	25126	27734	7.2%	3149	0.125
Part. 7	25528	28181	7.3%	3175	0.125
Part. 8	25236	27847	7.5%	3067	0.125
Sum of part.	201900	222939	6.6%	26720	1.000

4.2 Examining the effect of the turbulent dispersion force

At the beginning stage of the model validation, a too fast radial spreading of bubbles at lower measurement levels was observed in the numerical simulation. This led to the idea that the FAD model (Burns et al., 2004; Shi et al., 2005) might give a overly strong turbulence dispersion force. In order to have a detailed check of this issue, two calculations were carried out using a model coefficient $CTD = 0.5$ and 1.0, respectively. Here the model coefficient CTD is a factor used to adjust the turbulence dispersion force and should be distinguished from the so-called turbulence dispersion force coefficient C_{TD}.

For both calculations, a uniform volume fraction distribution was assumed for the liquid at the inlet together with a $1/7$-th power inlet velocity profile $U_{in} = 1.224U_0\,(1-r^*)^{1/7}$, where U_0 is the mean velocity and $r^* = 2r/D$ the dimensionless radial coordinate. The radial velocity was assumed to be null. In addition, a medium turbulence intensity (5%) was assigned there. In both calculations a model coefficient $FB = 1.0$ was applied for the bubble breakup model and a coefficient $FC = 0.5$ for the coalescence model.

The convergence information is given below. It is observed that the group size fraction equation seems to converge slower than the other equations. Both calculations were started from an OUTER LOOP ITERATION =21752, based on an initial result file obtained for the same test case but assuming uniform size fraction distribution at the gas injection. The physical time in the case $CTD = 0.5$ is equal to $(40253-21751)\times 0.0005 = 9.251$ [s] and in the case $CTD = 1.0$ equal to $(37232-21751)\times 0.0005 = 7.7405$ [s]. With reference to the superficial velocity of the liquid phase $U_{\ell,sup} = 1.017$ m/s, the results are valid for the full pipe in the case of $CTD = 0.5$ and are valid in the section within a distance 7.7 meters away from the gas injection.

```
      CTD1 = 0.5      CTD2 = 0.5
%=====================================================================
 OUTER LOOP ITERATION =40253 ( 5652) CPU SECONDS = 5.650E+07 (5.069E+06)
 ---------------------------------------------------------------------
 |       Equation       | Rate | RMS Res | Max Res |  Linear Solution |
 +----------------------+------+---------+---------+------------------+
 | U-Mom-Air1           | 0.65 | 7.1E-09 | 2.2E-06 |       8.2E-08  OK|
 | V-Mom-Air1           | 0.63 | 6.6E-09 | 1.9E-06 |       1.8E-07  OK|
 | W-Mom-Air1           | 0.92 | 2.0E-09 | 6.3E-07 |       5.6E-07  OK|
 | U-Mom-Air2           | 1.00 | 6.5E-10 | 4.0E-08 |       2.5E-03  OK|
 | V-Mom-Air2           | 1.05 | 1.8E-10 | 1.2E-08 |       6.1E-03  OK|
 | W-Mom-Air2           | 0.98 | 6.5E-10 | 4.2E-08 |       5.7E-04  OK|
 | U-Mom-Water          | 1.10 | 3.6E-06 | 9.9E-04 |       4.5E-05  OK|
 | V-Mom-Water          | 1.12 | 3.3E-06 | 8.7E-04 |       1.2E-04  OK|
 | W-Mom-Water          | 1.13 | 1.6E-06 | 2.9E-04 |       1.8E-05  OK|
 | P-Vol                | 0.39 | 2.3E-07 | 2.1E-05 | 10.2  2.3E-04  OK|
 +----------------------+------+---------+---------+------------------+
 | Mass-Air1            | 1.00 | 1.8E-04 | 2.7E-03 |  7.1  1.6E-05  OK|
 | Mass-Air2            | 1.00 | 3.0E-05 | 4.7E-04 |  7.1  1.6E-04  OK|
 | Mass-Water           | 1.00 | 1.5E-04 | 1.9E-02 |  7.3  4.3E-10  OK|
 +----------------------+------+---------+---------+------------------+
 | Sizfrc-Group 1       | 0.97 | 1.3E-03 | 2.2E-01 |  7.0  7.7E-08  OK|
 | Sizfrc-Group 2       | 0.98 | 8.8E-04 | 9.0E-02 |  7.0  5.5E-08  OK|
 | Sizfrc-Group 3       | 0.95 | 4.7E-04 | 5.0E-02 |  7.0  4.2E-08  OK|
 | Sizfrc-Group 4       | 0.97 | 2.8E-04 | 2.8E-02 |  7.0  1.7E-08  OK|
 | Sizfrc-Group 5       | 1.05 | 3.9E-04 | 5.6E-02 |  7.0  8.9E-09  OK|
 | Sizfrc-Group 6       | 1.01 | 4.5E-04 | 6.4E-02 |  7.0  1.2E-08  OK|
 | Sizfrc-Group 7       | 0.89 | 7.0E-04 | 1.1E-01 |  7.0  4.0E-08  OK|
 | Sizfrc-Group 8       | 0.85 | 9.1E-04 | 1.7E-01 |  7.0  7.5E-08  OK|
 | Sizfrc-Group 9       | 0.99 | 1.1E-02 | 2.7E-01 |  7.0  1.1E-08  OK|
 | Sizfrc-Group 10      | 0.99 | 1.1E-02 | 2.6E-01 |  7.0  9.3E-09  OK|
 | Sizfrc-Group 11      | 0.99 | 1.0E-02 | 2.6E-01 |  7.0  3.1E-09  OK|
 | Sizfrc-Group 12      | 0.99 | 1.0E-02 | 2.5E-01 |  7.0  5.4E-09  OK|
```

```
| Sizfrc-Group 13      | 0.99 | 9.9E-03 | 2.5E-01 |  7.0  2.0E-09  OK|
| Sizfrc-Group 14      | 0.99 | 9.6E-03 | 2.4E-01 |  7.0  7.2E-09  OK|
| Sizfrc-Group 15      | 0.99 | 9.3E-03 | 2.4E-01 |  7.0  1.2E-09  OK|
| Sizfrc-Group 16      | 0.99 | 9.0E-03 | 2.3E-01 |  7.0  6.8E-09  OK|
| Sizfrc-Group 17      | 0.99 | 8.7E-03 | 2.2E-01 |  7.0  9.6E-10  OK|
| Sizfrc-Group 18      | 0.99 | 8.4E-03 | 2.2E-01 |  7.0  3.6E-09  OK|
| Sizfrc-Group 19      | 0.99 | 8.0E-03 | 2.1E-01 |  7.0  4.2E-10  OK|
| Sizfrc-Group 20      | 0.99 | 7.6E-03 | 2.0E-01 |  7.0  2.4E-10  OK|
| Sizfrc-Group 21      | 0.99 | 7.1E-03 | 1.9E-01 |  7.0  4.0E-09  OK|
+----------------------+------+---------+---------+------------------+
| K-TurbKE-Water       | 1.00 | 5.3E-06 | 8.6E-05 |  6.7  2.4E-06  OK|
| O-TurbFreq-Water     | 1.00 | 8.4E-07 | 8.3E-05 |  7.9  4.8E-06  OK|


     CTD1 = 1.0       CTD2 = 1.0
=======================================================================
 OUTER LOOP ITERATION =37232 ( 3250) CPU SECONDS = 5.279E+07 (4.989E+06)
 -----------------------------------------------------------------------
 |       Equation       | Rate | RMS Res | Max Res |  Linear Solution |
 +----------------------+------+---------+---------+------------------+
 | U-Mom-Air1           | 0.58 | 7.8E-09 | 2.8E-06 |       1.5E-05  OK|
 | V-Mom-Air1           | 0.61 | 7.5E-09 | 2.8E-06 |       3.0E-05  OK|
 | W-Mom-Air1           | 1.14 | 6.8E-09 | 8.5E-07 |       3.1E-04  OK|
 | U-Mom-Air2           | 1.00 | 2.9E-07 | 1.4E-05 |       5.6E-03  OK|
 | V-Mom-Air2           | 1.00 | 1.1E-07 | 5.7E-06 |       4.0E-03  OK|
 | W-Mom-Air2           | 1.00 | 1.4E-06 | 6.6E-05 |       2.3E-03  OK|
 | U-Mom-Water          | 0.90 | 5.1E-06 | 4.7E-04 |       5.0E-03  OK|
 | V-Mom-Water          | 0.72 | 2.3E-06 | 4.4E-04 |       1.3E-02  OK|
 | W-Mom-Water          | 1.00 | 8.7E-06 | 4.4E-04 |       1.1E-02  OK|
 | P-Vol                | 1.06 | 1.1E-04 | 4.4E-03 | 10.2  4.0E-03  OK|
 +----------------------+------+---------+---------+------------------+
 | Mass-Air1            | 1.08 | 3.3E-02 | 1.1E+00 |  7.0  1.1E-05  OK|
 | Mass-Air2            | 0.99 | 6.7E-03 | 2.3E-01 |  7.0  7.4E-05  OK|
 | Mass-Water           | 1.00 | 2.6E-04 | 1.8E-02 |  7.3  3.5E-09  OK|
 +----------------------+------+---------+---------+------------------+
 | Sizfrc-Group 1       | 1.00 | 1.6E-03 | 6.1E-02 |  7.0  2.4E-06  OK|
 | Sizfrc-Group 2       | 1.00 | 1.2E-03 | 3.4E-02 |  7.0  2.0E-06  OK|
 | Sizfrc-Group 3       | 1.00 | 6.5E-04 | 2.1E-02 |  7.0  1.8E-06  OK|
 | Sizfrc-Group 4       | 1.00 | 4.4E-04 | 2.8E-02 |  7.0  9.4E-07  OK|
 | Sizfrc-Group 5       | 1.00 | 5.2E-04 | 1.7E-02 |  7.0  6.9E-07  OK|
 | Sizfrc-Group 6       | 1.00 | 6.0E-04 | 2.2E-02 |  7.0  3.2E-07  OK|
 | Sizfrc-Group 7       | 1.00 | 9.4E-04 | 3.9E-02 |  7.0  1.9E-06  OK|
 | Sizfrc-Group 8       | 1.00 | 1.2E-03 | 6.1E-02 |  7.0  3.0E-06  OK|
 | Sizfrc-Group 9       | 1.00 | 8.1E-03 | 2.7E-01 |  7.0  9.2E-07  OK|
 | Sizfrc-Group 10      | 1.00 | 8.0E-03 | 2.7E-01 |  7.0  1.3E-06  OK|
 | Sizfrc-Group 11      | 1.00 | 7.8E-03 | 2.6E-01 |  7.0  1.6E-06  OK|
 | Sizfrc-Group 12      | 1.00 | 7.6E-03 | 2.6E-01 |  7.0  1.5E-06  OK|
 | Sizfrc-Group 13      | 1.00 | 7.5E-03 | 2.5E-01 |  7.0  2.9E-06  OK|
 | Sizfrc-Group 14      | 1.00 | 7.3E-03 | 2.4E-01 |  7.0  4.7E-07  OK|
```

Sizfrc-Group 15	1.00	7.1E-03	2.4E-01	7.0	1.4E-06	OK
Sizfrc-Group 16	1.00	6.9E-03	2.3E-01	7.0	7.4E-07	OK
Sizfrc-Group 17	1.00	6.7E-03	2.3E-01	7.0	1.2E-06	OK
Sizfrc-Group 18	1.00	6.4E-03	2.2E-01	7.0	9.7E-07	OK
Sizfrc-Group 19	1.00	6.2E-03	2.1E-01	7.0	7.4E-07	OK
Sizfrc-Group 20	1.00	5.8E-03	2.0E-01	7.0	6.4E-07	OK
Sizfrc-Group 21	1.00	5.4E-03	1.9E-01	7.0	7.3E-08	OK
K-TurbKE-Water	1.00	1.7E-05	4.9E-04	6.7	2.7E-03	OK
O-TurbFreq-Water	1.00	2.9E-06	1.3E-04	7.9	6.8E-03	OK

4.2.1 Radial profile of the gas volume fraction

Comparison of the numerical results and experimental data for the radial distribution of the gas volume fraction is presented in Figs. 4.1 and 4.2 for the total gas phase and for each velocity group. Good agreements with the measurement data can be observed for the total gas volume fraction at levels from A to J in the case $CTD = 0.5$. Nevertheless, the agreements become very poor in region far away from the injection plane. The radial spreading of the gas phase seems to be too slow and consequently no fully developed flow was predicted along the entire pipe length using this reduced value for the turbulence dispersion force. In contrast, a fully developed flow was predicted and fairly good agreements with experimental data were obtained at levels of larger heights, e.g. M, P, R, in the case $CTD = 1.0$, despite that too strong radial transportation of the gas phase was observed at lower levels. For this reason, the default model coefficient in CFX10.0, $CTD = 1.0$, was chosen in all the other numerical simulations. In addition, the bubble coalescence is too strong in both cases, resulting in too many gas in the the velocity group of larger bubbles (Air2) and too little in the group of smaller bubbles (Air1) compared with the measurement data. The results for the size distribution are presented in Figs 4.3 and 4.4 in section 4.2.2.

4.2.2 Bubble size fraction distribution

The results for the bubble size fraction distribution function are demonstrate in Figs. 4.3 and 4.4. The mean value over the cross pipe section,as is defined below, are plotted.

$$h(d_j) = \mathrm{d}\overline{\alpha(x)}/dx|_{x=d_j},\ \overline{\alpha(d_j)} = \int_0^R \alpha(r, d_j)\, 2\pi\, r\, \mathrm{d}r/(\pi\, R^2) \tag{15}$$

Obviously, overly strong coalescence was obtained in both calculations compared with the measurement data. This occurs in simulation even from the level A with a distance 0.221 m over the gas injection plane. The breakup is also too strong compared with the measurement data. Different from the experimental observation, the initial size distribution loses shape soon after injection in simulation. However, a stronger turbulence dispersion force seems to prevent the strong trend of coalesence to some extent at levels A and D. With reference to Fig. 4.1, the radial transportation of the bubbles is faster in the case $CTD = 1$. This leads to a sooner reduction of the peak gas concentration and hence decreases the coalescence rate in the region. Considering the

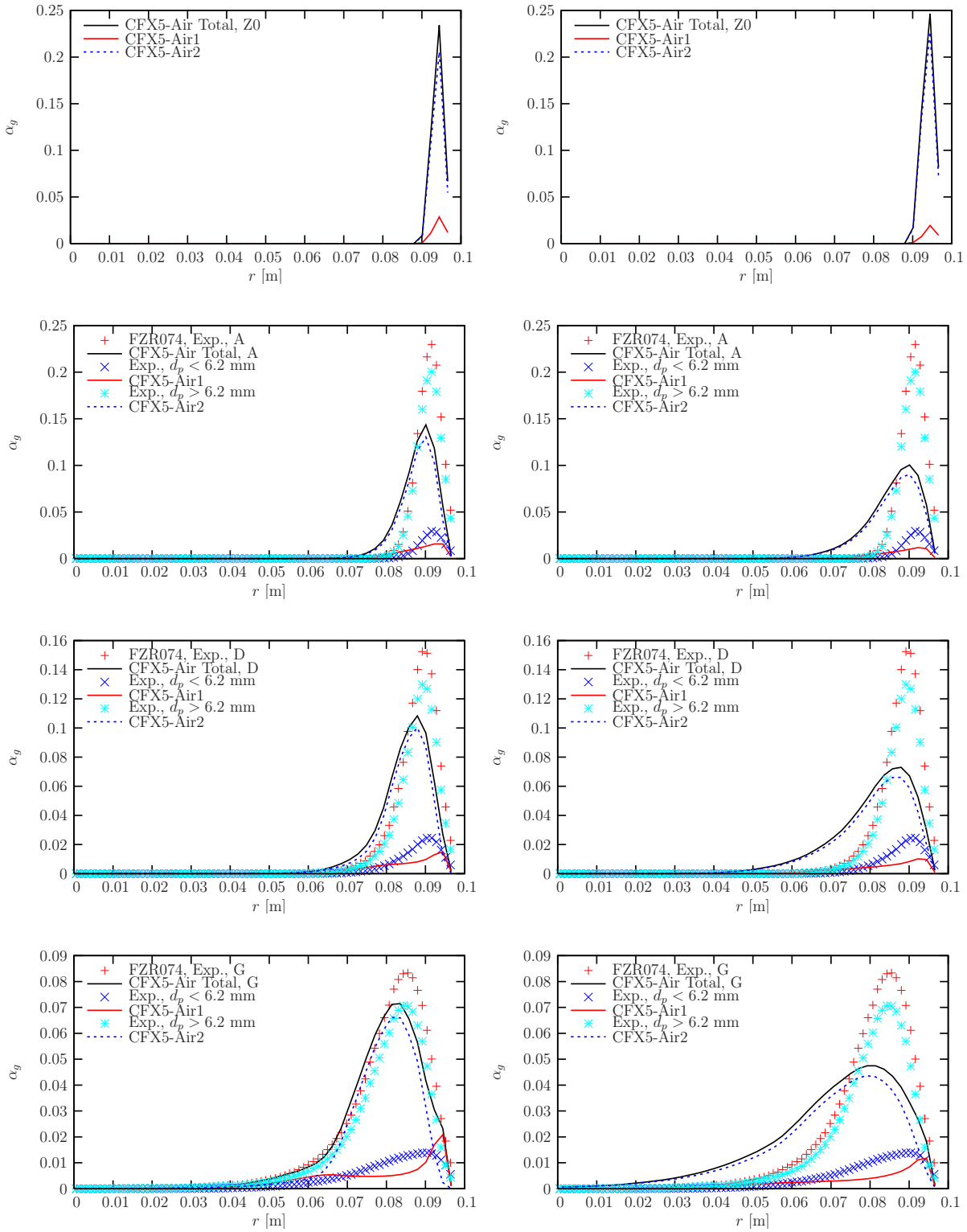

Fig. 4.1: Comparison of experimental and numerical results for the radial profile of the gas volume fraction. Test case 074. The measurement planes denoted by $Z0$, A, D, G, J, M, P and R correspond to a distance 0.0, 0.221, 0.494, 1.438, 2.481, 4.417, 7.688 and 7.802 m, respectively, away from the gas injection. Left: $CTD = 0.5$; Right: $CTD = 1.0$.

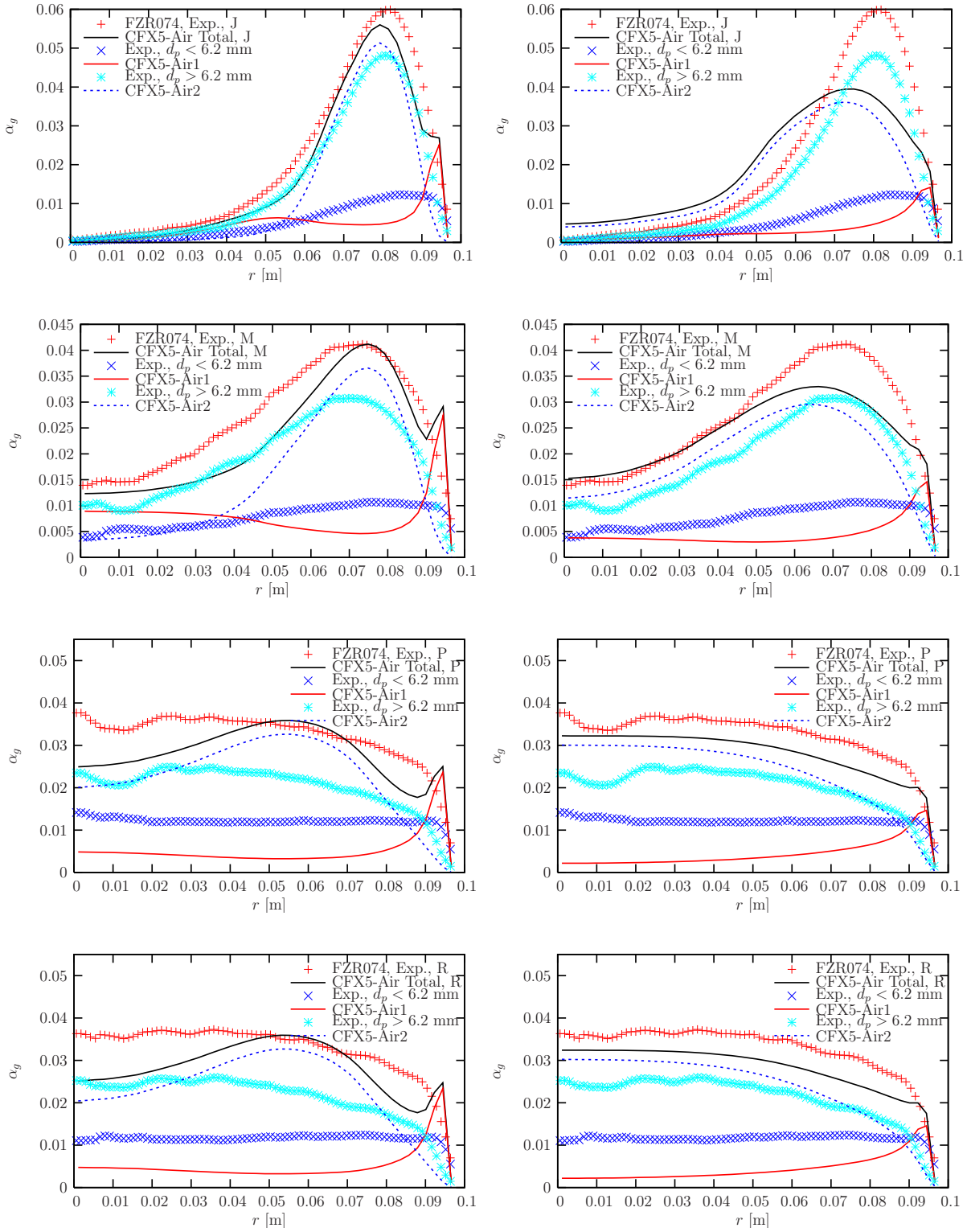

Fig. 4.2: Comparison of experimental and numerical results for the radial profile of the gas volume fraction. Test case 074, continued.

over-predicted coalescence behavior, reduced values were applied for the coalescence model (Prince and Blanch, 1990) in the simulations carried out later. The results are presented in section 4.3.

4.2.3 The gas velocity profile

Here and in the following text, the vertical component of the volume-weighted velocity was adopted for the comparison. The definition is as follows

$$w = \frac{(\alpha + \epsilon)\, w_g}{\alpha + \epsilon} \tag{16}$$

where $\epsilon = 10^{-4}$ is a small value to avoid a null denometer in locations where $\alpha = 0$, namely where there exists no gas.

The vertical gas velocity profiles at various heights along the pipe predicted by using $CTD = 0.5$ and $CTD = 1.0$ are displayed in Figs. 4.5 and 4.6. The corresponding experimental data are also plotted for comparison. Very good agreements between the numerical results and the measurement data can be observed. This implies that the drag force model applied here is suitable for the present flow of low gas concentration. The deviations in the spreading edge of the gas phase or in the core region where the gas volume fraction is extremely small are not critical and can be reduced by choosing a suitable value for ϵ of Eq. (16). In both calculations, fully developed velocity profiles were predicted at planes close to the upper end of the pipe. It was also obaserved that the lateral spreading of the gas phase is much faster by adopting the CFX10.0 default model coefficient $CTD = 1.0$.

4.3 Calibration of the coalescence and breakup model

Considering the over-predicted coalescence behavior in the numerical results presented in section 4.2, a smaller model coefficient rather than $FC = 0.50$ has to be applied for the coalescence model. Moreover, both the coalescence and breakup model coefficient need to be calibrated. For that purpose, a number of numerical experiments using various combination of model coefficients were performed. As the evaluation criterion, the averged bubble size fraction distributions over various cross-sections [Eq. (15)] were compared with the corresponding experimental data.

The simulations were carried out by assigning the fully developed flow conditions at the inlet. The original FAD turbulence dispersion force model ($CTD = 1.0$) was applied considering the fairly good agreements with experimental data observed in the fully developed flow region based on this value (see Fig. 4.2).

From a number of calculations carried out, we choose two cases, one based on $FB = 0.05$ and $FC = 0.01$ and the other on $FB = 1.0$ and $FC = 0.01$, for the presentation. The results for the vertical gas velocity (16) from both simulations are quite similar to each other. Hence only those for the case $FB = 1.0$ and $FC = 0.01$ are presented here. The radial velocity profiles of the gas phase at various measurement levels from the simulation and measurement data are displayed in Fig. 4.7 for comparison. The numerical results for each bubble velocity group and for the liquid phase are also included. Again remarkabbly good agreements between the simulation and measurement can be observed. In addition, it is noted that the liquid velocity profiles

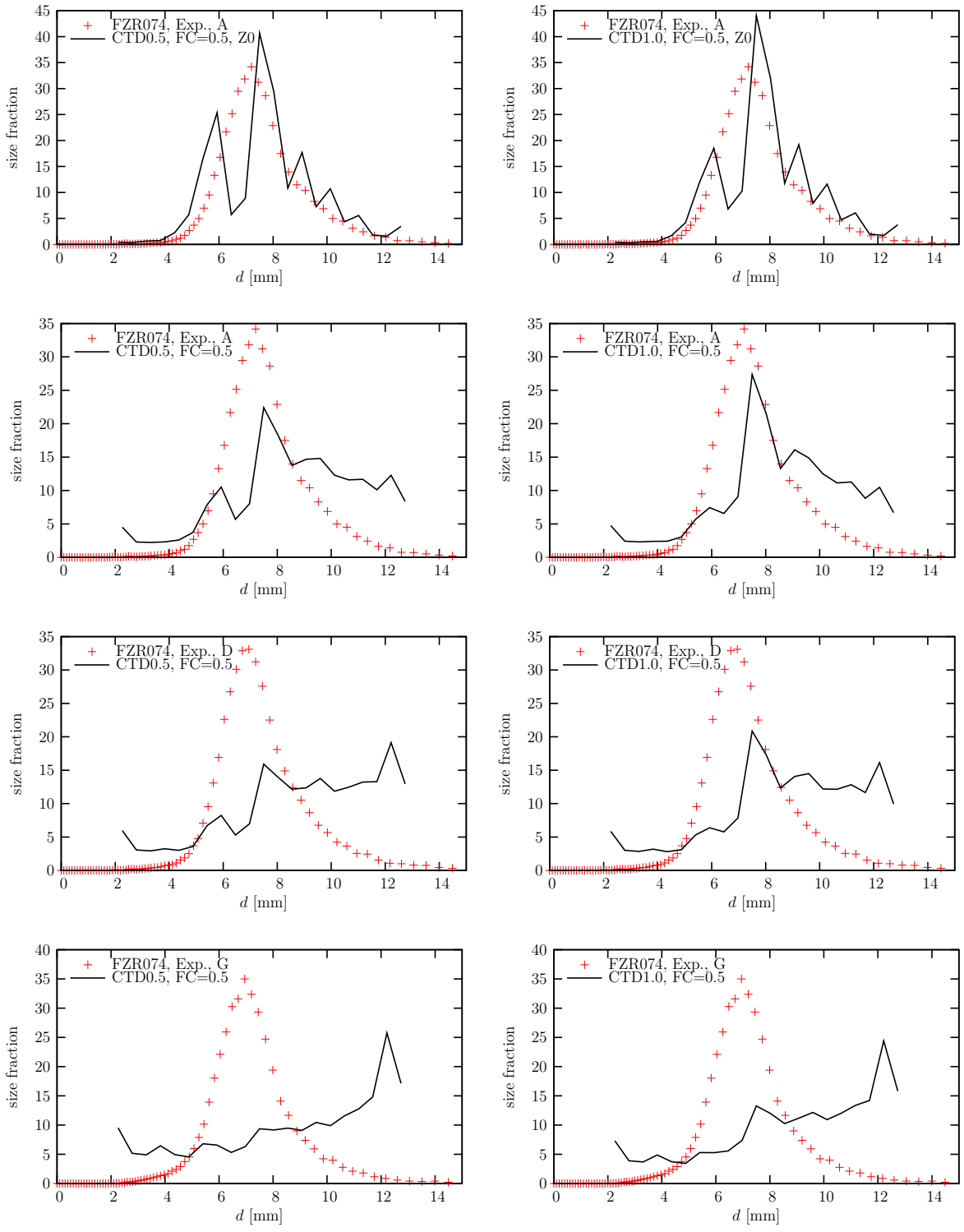

Fig. 4.3: Comparison of experimental and numerical results for the mean size distribution function over the corss-sections. Test case 074. The measurement planes denoted by $Z0$, A, D, G, J, M, P and R correspond to a distance 0.0, 0.221, 0.494, 1.438, 2.481, 4.417, 7.688 and 7.802 m, respectively, away from the gas injection. Left: $CTD = 0.5$; Right: $CTD = 1.0$, continued.

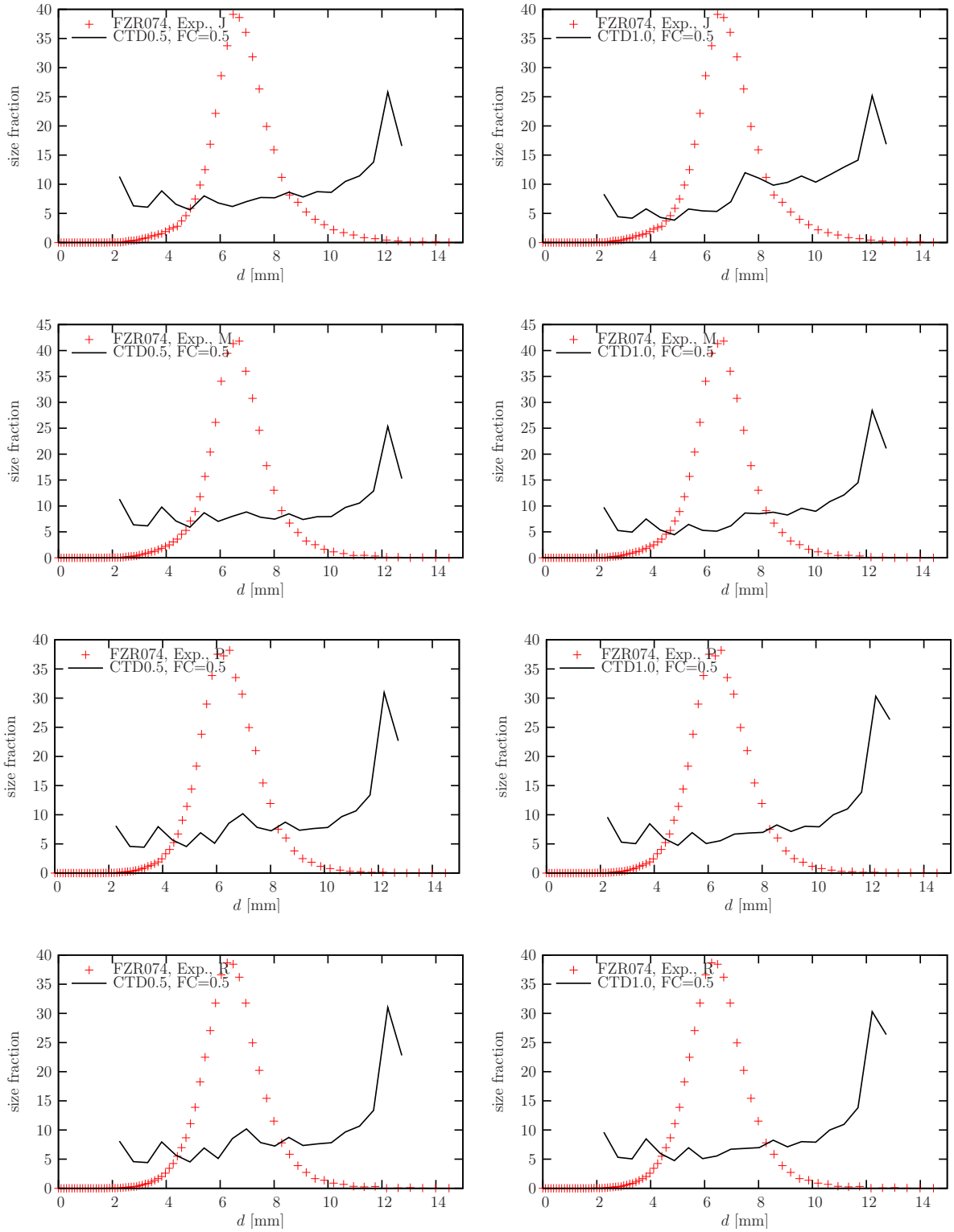

Fig. 4.4: Comparison of experimental and numerical results for the radial velocity profile of the gas phase. Test case 074, continued.

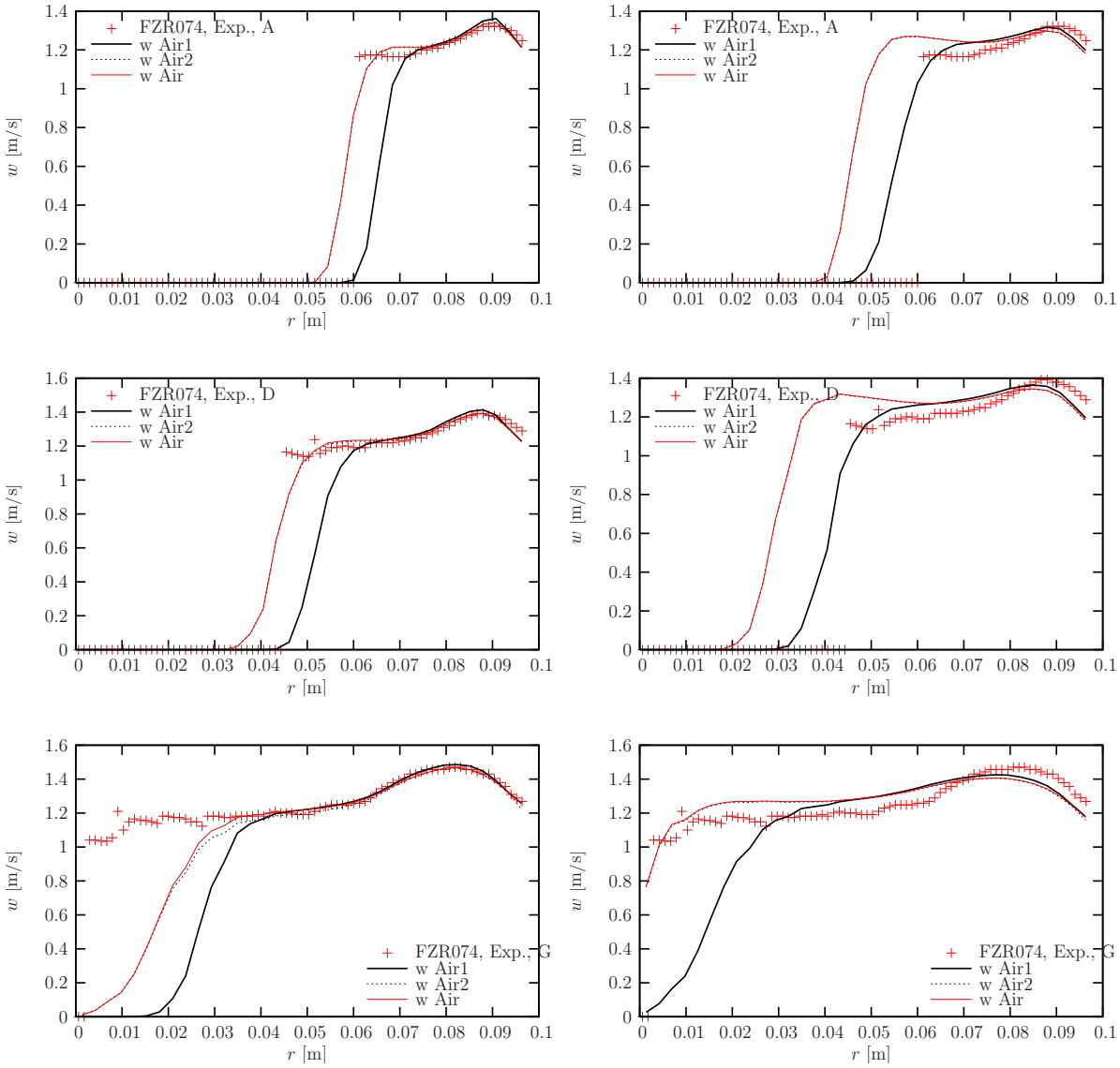

Fig. 4.5: Comparison of experimental and numerical results for the radial velocity profile of the gas phase. Test case 074. The measurement planes denoted by $Z0$, A, D, G, J, M, P and R correspond to a distance 0.0, 0.221, 0.494, 1.438, 2.481, 4.417, 7.688 and 7.802 m, respectively, away from the gas injection. Left: $CTD = 0.5$; Right: $CTD = 1.0$.

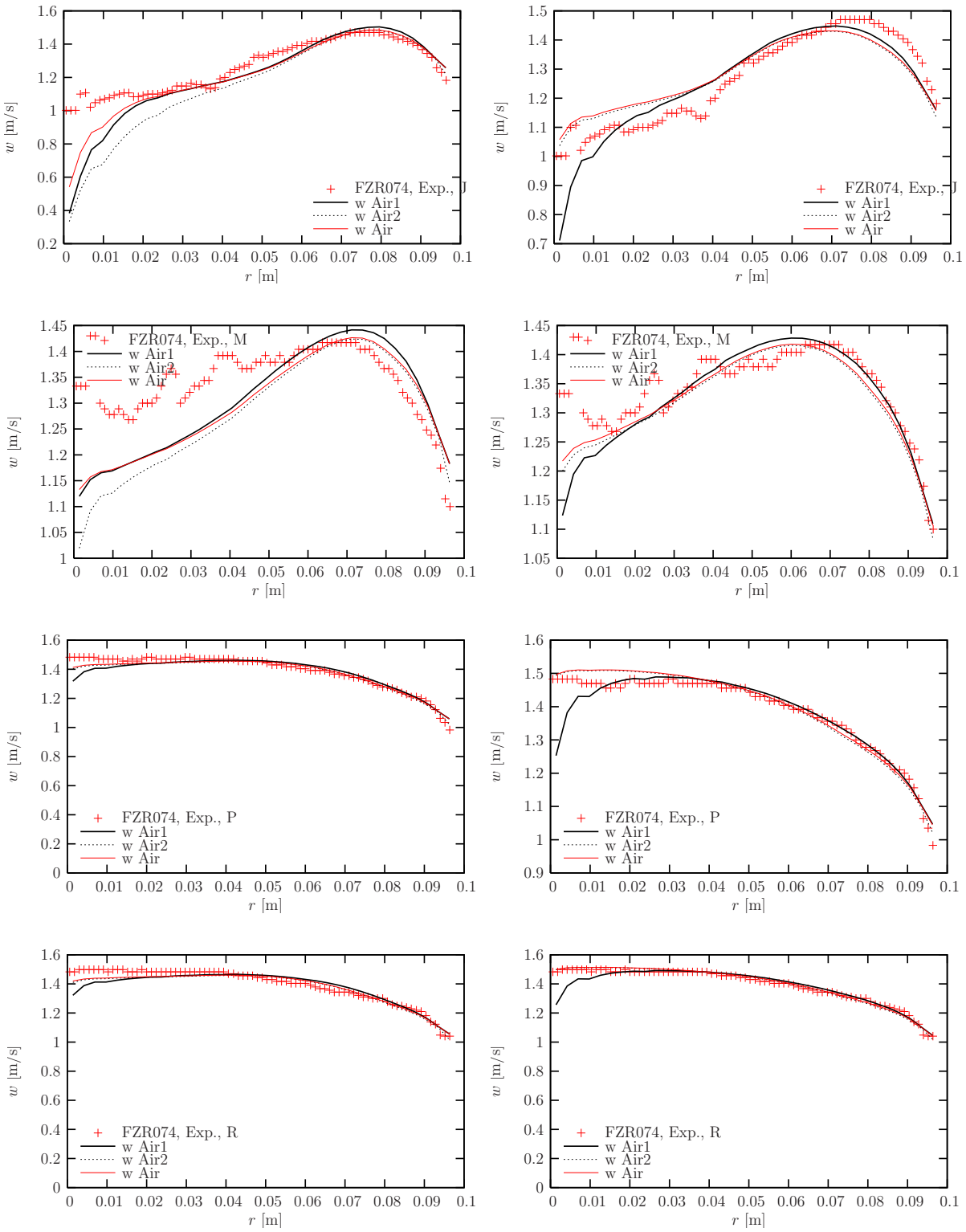

Fig. 4.6: Comparison of experimental and numerical results for the radial velocity profile of the gas phase. Test case 074, Left: $CTD = 0.5$; Right: $CTD = 1.0$, continued.

are strongly distorted by the evlolution of the gas in the pipe. At the upper end of the pipe a fully-developed velocity profile become established again for both phases.

The results for the radial profiles of the volume fraction and the average bubble size fraction distribution (15) over the cross sections together with the corresponding measurement data are demonstrated in Figs. 4.8 and 4.9 for the case based on $FB = 0.05$ and $FC = 0.01$ and in Figs. 4.10 and 4.11 for the case using $FB = 1.0$ and $FC = 0.01$. It is observed that the bubble breakup rate was under-predicted while the coalescence rate was overly predicted in the simulation applying the coefficient set, $FB = 0.05$ and $FC = 0.01$. In contrast, fairly good agreements were obtained for both the radial profile of the gas volume fraction and the average bubble size fraction distribution over the cross section by applying $FB = 1.0$ and $FC = 0.01$. These results indicate that the $N \times M$ MUSIG model is capable of predicting the evolution of the bubbly flow along the pipe despite the fact that some deviations from the measurement data are observed. It should be noted that the coalescence and breakup model is still in an inmature developing stage. The inaccuracy of these models should be mainly responsible for those deviations. The numerical results can be improved if a suitable breakup and coalescence model will be available.

5 The test case 107

5.1 Further details of the numerical settings

According to the measurement data, the bubble diameter can be restricted to the range 2 to 44mm. The discretization of the velocity and size group is described in Table 5.1.

The initial bubble size fraction distribution of the gas injected from the orifices, which was modeled by means of point mass source, is as follows

```
sfvalue1 =  0.83984/100.0
sfvalue2 = 2.02065/100.0
sfvalue3 = 2.36027/100.0
sfvalue4 = 2.57819/100.0
sfvalue5 = 2.63183/100.0
sfvalue6 = 2.83568/100.0
sfvalue7 = 3.03482/100.0
sfvalue8 = 3.52096/100.0
sfvalue9 = 4.05001/100.0
sfvalue10 = 6.1243/100.0
sfvalue11 = 7.24006/100.0
sfvalue12 = 8.90801/100.0
sfvalue13 = 9.17488/100.0
sfvalue14 = 10.2471/100.0
sfvalue15 = 10.5223/100.0
sfvalue16 = 9.30731/100.0
sfvalue17 = 7.34701/100.0
sfvalue18 = 4.05638/100.0
sfvalue19 = 1.89827/100.0
sfvalue20 = 0.942432/100.0
sfvalue21 = 0.35974/100.0
```

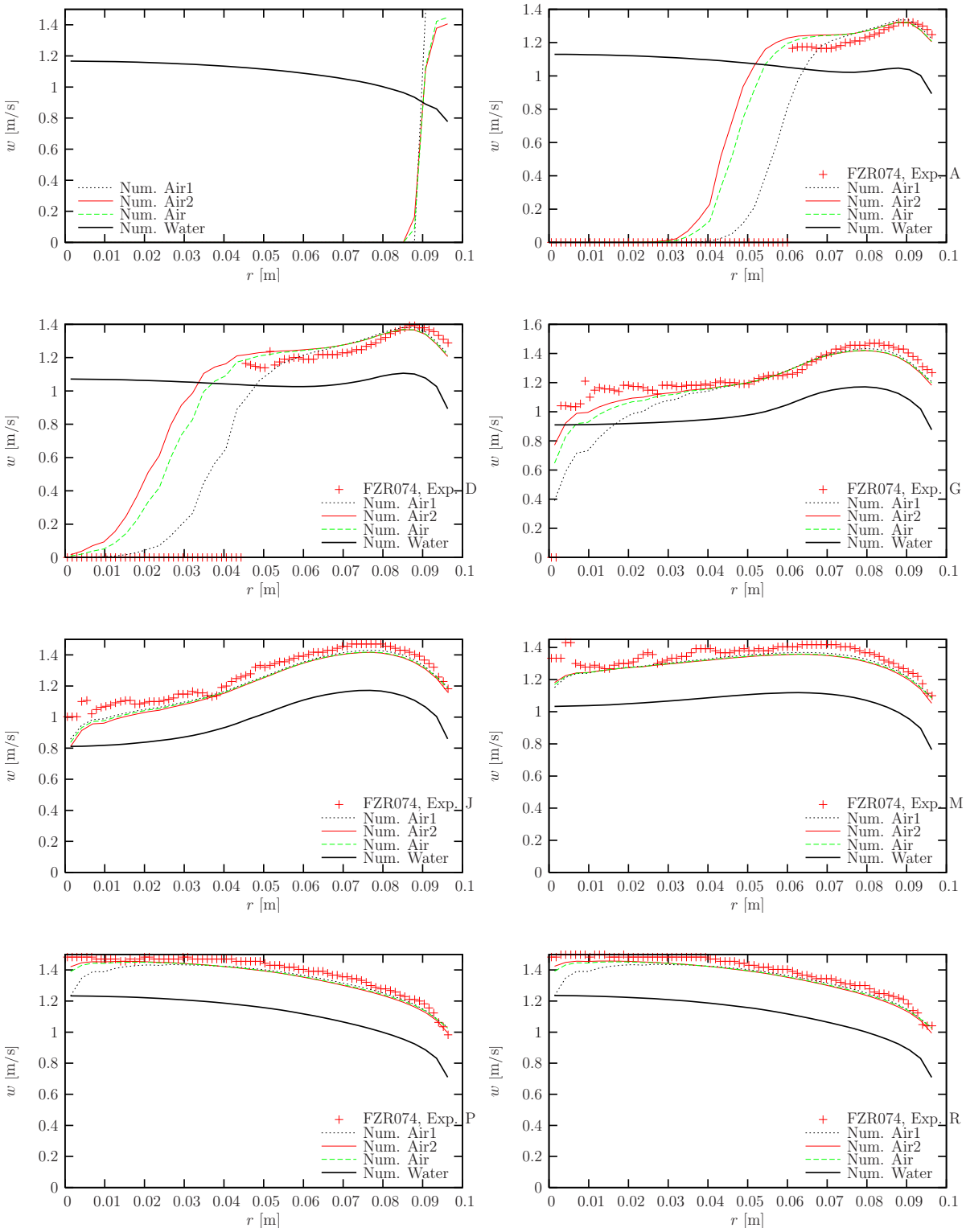

Fig. 4.7: Comparison of the predicted and measured radial gas velocity profiles. Test case 074, using $FB = 1.0$ and $FC = 0.01$.

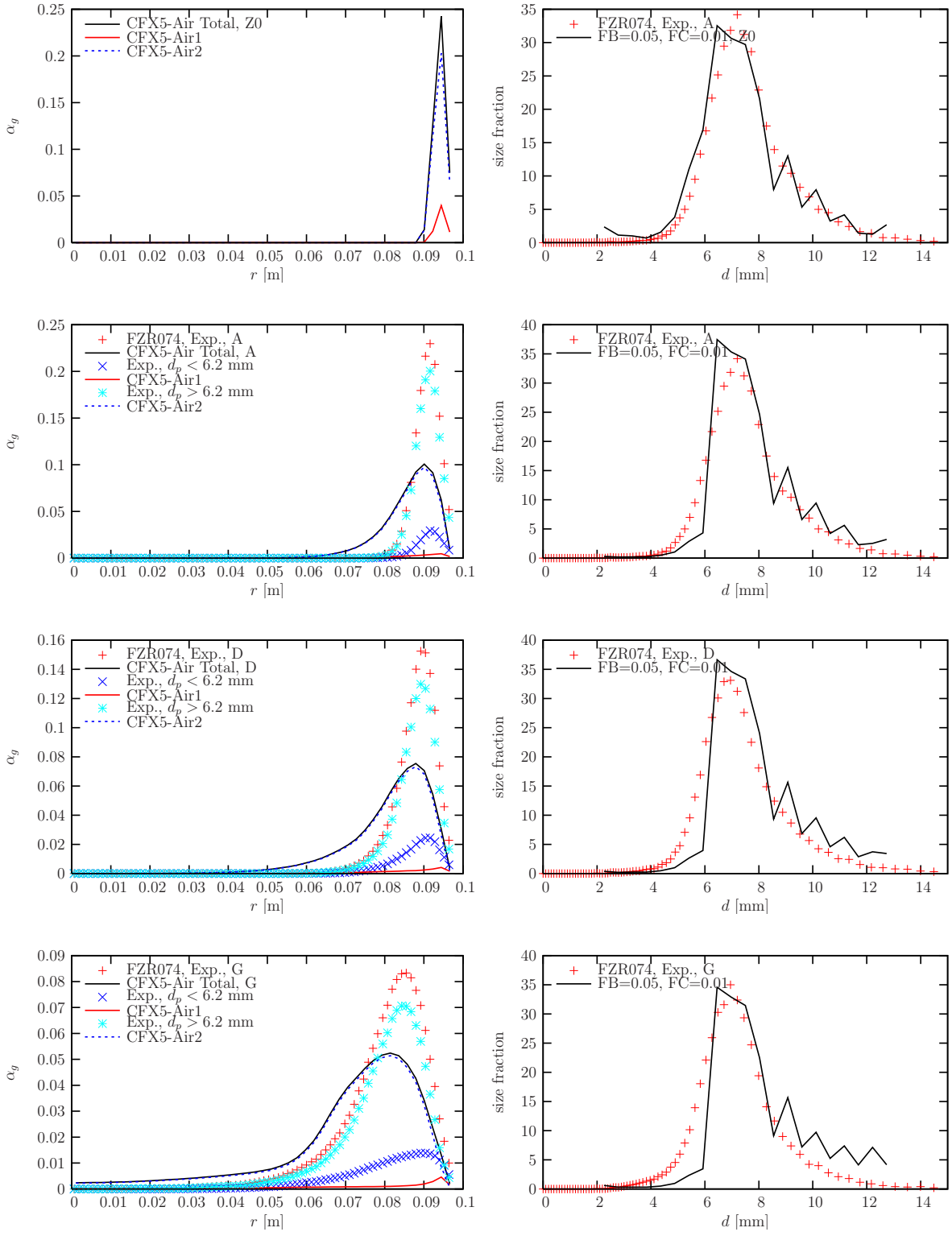

Fig. 4.8: Comparison of experimental and numerical results for the radial velocity and gas volume fraction profile and the average bubble size fraction distribution. Test case 074, with $FB = 0.05$ and $FC = 0.01$.

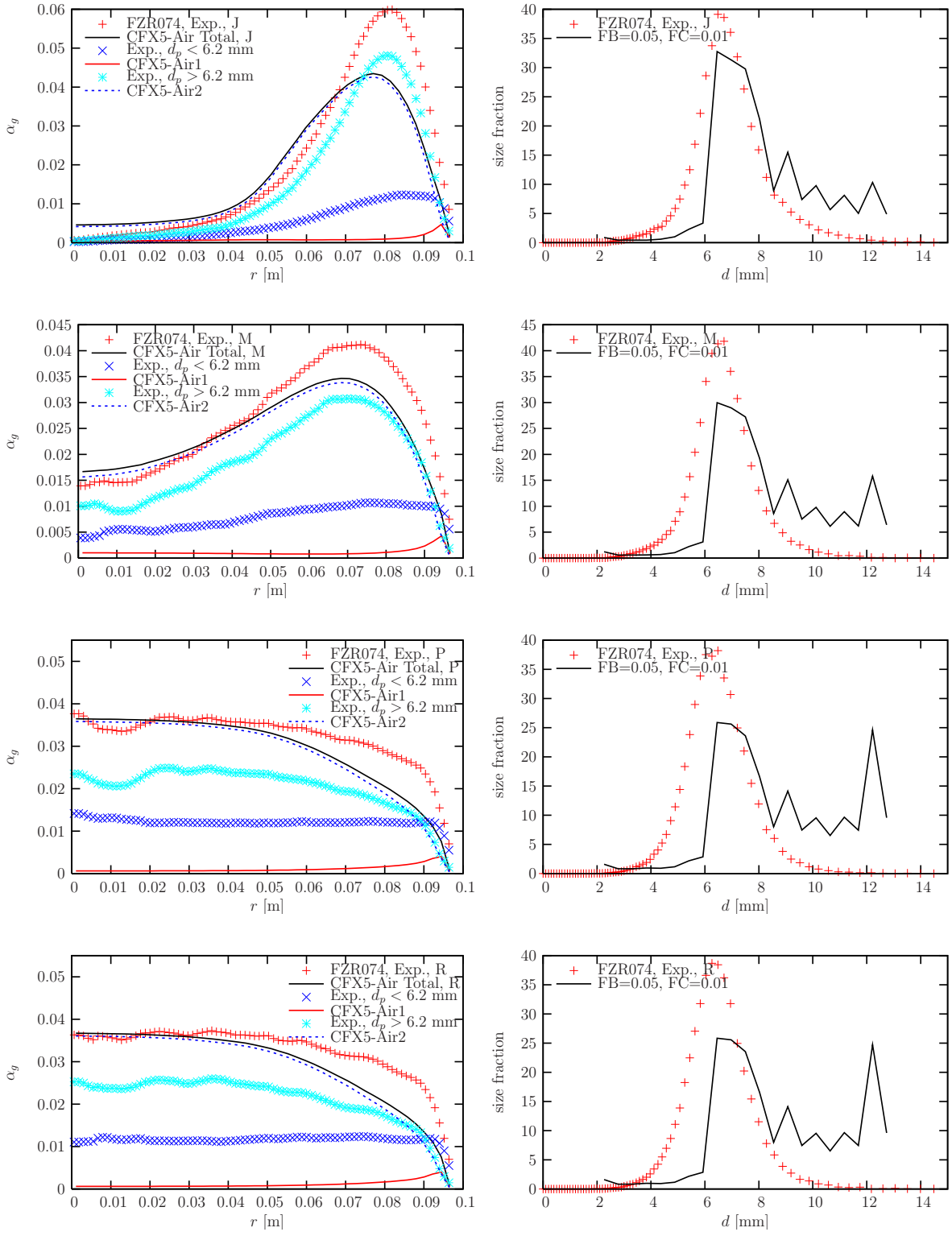

Fig. 4.9: Comparison of experimental and numerical results for the radial velocity and gas volume fraction profile and the average bubble size fraction distribution. Test case 074, $FB = 0.05$ and $FC = 0.01$, continued.

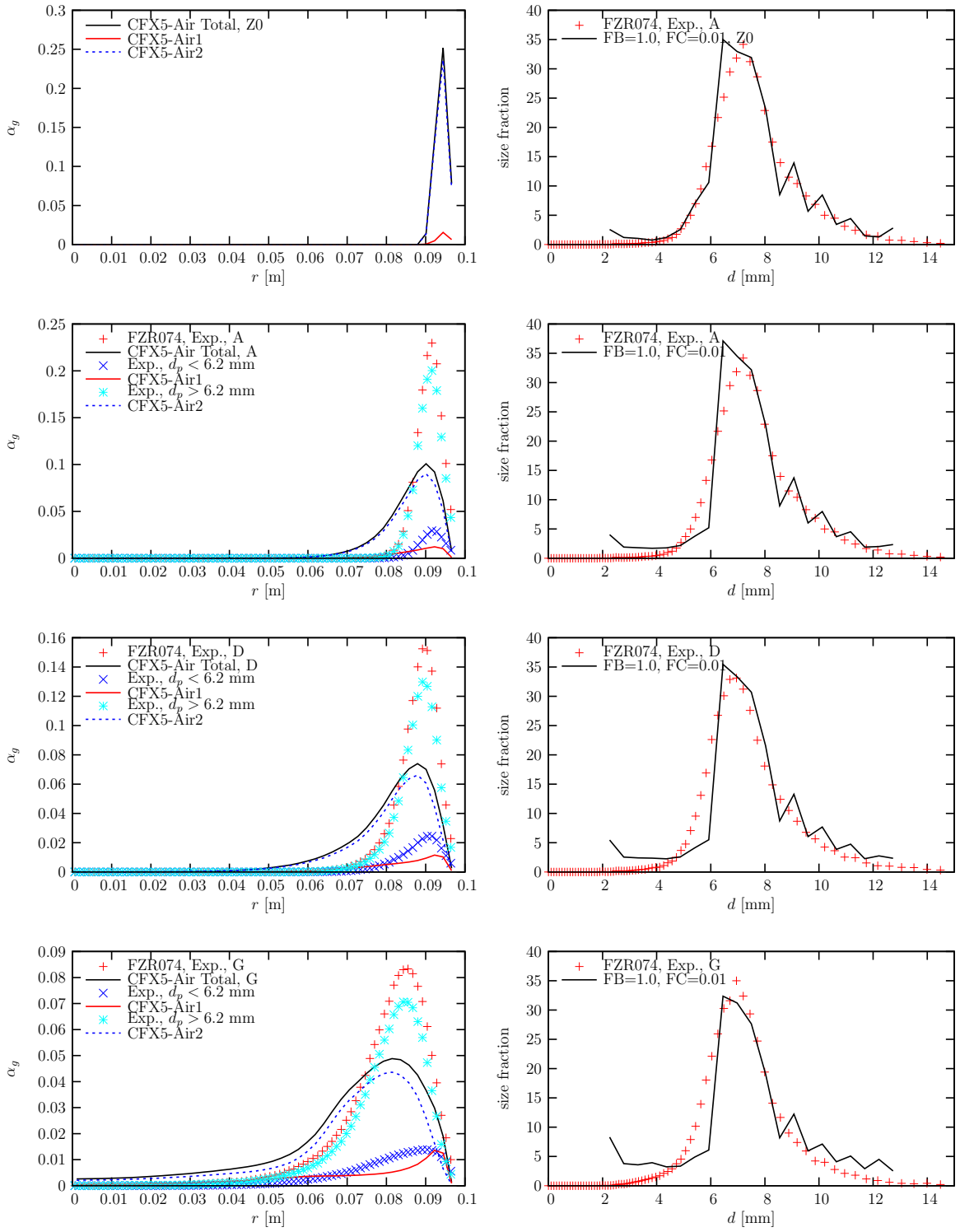

Fig. 4.10: Comparison of experimental and numerical results for the radial velocity and gas volume fraction profile and the average bubble size fraction distribution. Test case 074, $FB = 1.0$ and $FC = 0.01$.

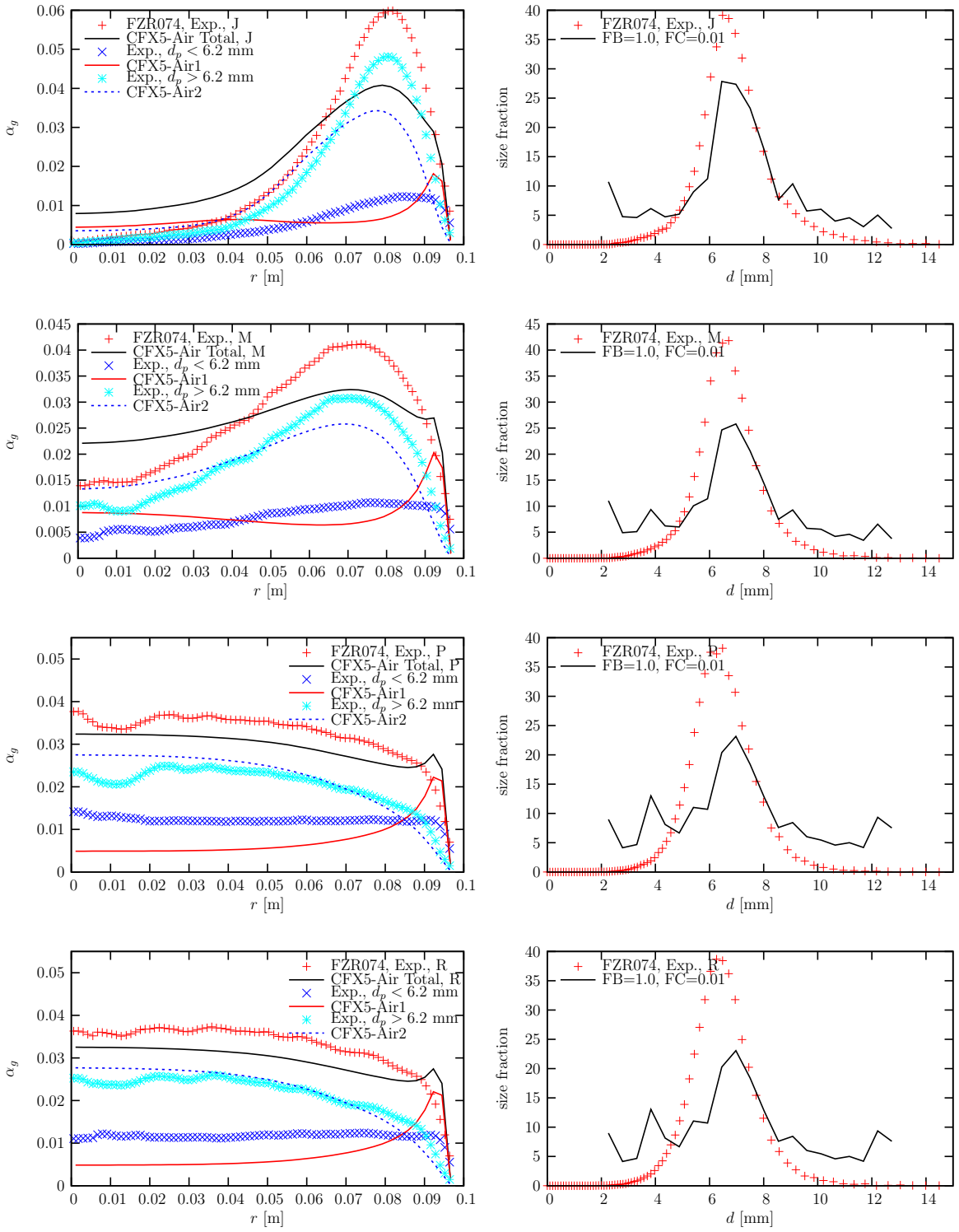

Fig. 4.11: Comparison of experimental and numerical results for the radial velocity and gas volume fraction profile and the average bubble size fraction distribution. Test case 074, $FB = 1.0$ and $FC = 0.01$, continued.

Group	Polydispersed Fluid	Diameter	Mass
Group 1	Air1	3.0000E-03	1.6753E-08
Group 2	Air1	5.0000E-03	7.7558E-08
Group 3	Air2	7.0000E-03	2.1282E-07
Group 4	Air2	9.0000E-03	4.5232E-07
Group 5	Air2	1.1000E-02	8.2584E-07
Group 6	Air2	1.3000E-02	1.3632E-06
Group 7	Air2	1.5000E-02	2.0941E-06
Group 8	Air2	1.7000E-02	3.0483E-06
Group 9	Air2	1.9000E-02	4.2558E-06
Group 10	Air2	2.1000E-02	5.7461E-06
Group 11	Air2	2.3000E-02	7.5492E-06
Group 12	Air2	2.5000E-02	9.6948E-06
Group 13	Air2	2.7000E-02	1.2213E-05
Group 14	Air2	2.9000E-02	1.5133E-05
Group 15	Air2	3.1000E-02	1.8484E-05
Group 16	Air2	3.3000E-02	2.2298E-05
Group 17	Air2	3.5000E-02	2.6602E-05
Group 18	Air2	3.7000E-02	3.1428E-05
Group 19	Air2	3.9000E-02	3.6805E-05
Group 20	Air2	4.1000E-02	4.2763E-05
Group 21	Air2	4.3000E-02	4.9331E-05

Tab. 5.1: MUSIG fluid and group discretization, Test case 107.

The above data was defined according to the experimental bubble size fraction distribution measured for the gas injected at plane A with a distance of 0.221m from the wire mesh sensor.

In order to account for the effect of the high volume fraction on the bubble drag, the Grace drag model (Grace and Weber, 1982) was multiplied by a a factor α_g^n, where α_g^c is the local gas volume fraction. A value $c = -2$ was applied for the velocity group of small bubbles and $c = 2$ for the larger group. this is because the drag increases for small bubbles and decreases for large bubbles at high gas concentration. The unmodified FAD model was applied for the turbulence dispersion force, namely using $CTD = 1.0$. The superficial velocity for the liquid and the gas phase were inputed into the simulation through the following CEL expressions,

```
ug leer = 0.140 [m s^-1]
ul leer = 1.0167 [m s^-1]
```

The simulations were performed by applying the code CFX10.0 and using a time step d$t = 0.002$[s]. The other ccl settings and the convergence behaviour are similar to those given in section 4.1.

5.2 Results and discussion

The two sets of breakup and coalescence model coefficients, $FB = 1.0$ combined with $FC = 0.01$ and $FB = 0.05$ with $FC = 0.01$, adopted for the test case 074 were applied to the current test case. The results are discussed in section 5.2.1 and section 5.2.2, respectively. Another calculation based on $FB = 0.25$ and $FC = 0.01$ is also presented in section 5.2.3.

5.2.1 FB=1.0, FC=0.01

The comparisons of the numerical and experimental results for the radial profiles of the vertical gas velocity (left), of the gas volume fraction (middle) and the average bubble size fraction distribution (right) are presented in Fig. 5.1 for the case using $FB = 1.0$ and $FC = 0.01$. It is observed from the left column of the figure that the evolution of the gas velocity profile along the pipe was correctly predicted. Nevertheless, the deviations from the measurements are much larger than those observed in the test case 074, where the gas volume fraction in the pipe is low. This indicate that the effect of the high volume fraction on the drag force was not perfectly treated by the modifications to the Grace drag force model (Grace and Weber, 1982) mentioned above. The influence of the high gas concentration on the non-drag forces were not considered, which should also have contrinuted to the deviations from the measurement data.

The bubble breakup was overly pronounced in the numerical simulation, resulting in too many gas volume fraction in the smaller bubbles (Air1) and an over-predicted wall peak in the gas volume fraction profiles. In contrast, a fairly good agreements with the measurments were obtained in the test case 074 by using the same set of model coefficients (refer to Figs. 4.10 and. 4.11). On the other hand, the shape of the average bubble size fraction distribution over the cross section of level R, where the flow becomes fully developed, was correctly predicted.

5.2.2 FB=0.05, FC=0.01

The results based on $FB = 0.05$ and $FC = 0.01$ are presented in Fig. 5.2. The evolution of the gas volume fraction in the pipe was largely predicted using this set of model coefficients, despite that the bubble breakup and thus the volume fraction of the small bubbles were under predicted. Similar to the corresponding results of the test case 074, the avergae bubble size fraction distribution over the corss sections (e.g., level A and D) close to the gas injection level agrees quite well with the measurement data, whereas the numerical size fraction distribution are quite different from the experimental data at higher levels. Compared the present results with those results based on $FB = 0.1.0$ and $FC = 0.01$ (Fig. 5.1), one might be allowed to come to the conclusion that some breakup and coalescence mechnisms important for the present flow might haven't been iconsidered in the models applied here. As an work-around method, one might need to adopt a small coefficient for the breakup model in the flow region close to the gas injection and an increasing value with the increasing pipe height.

5.2.3 FB=0.25, FC=0.01

The results based on $FB = 0.05$ and $FC = 0.01$ are presented in Fig. 5.3. The radial volume fraction profiles from the numerical simulation agree remarkbaly well with

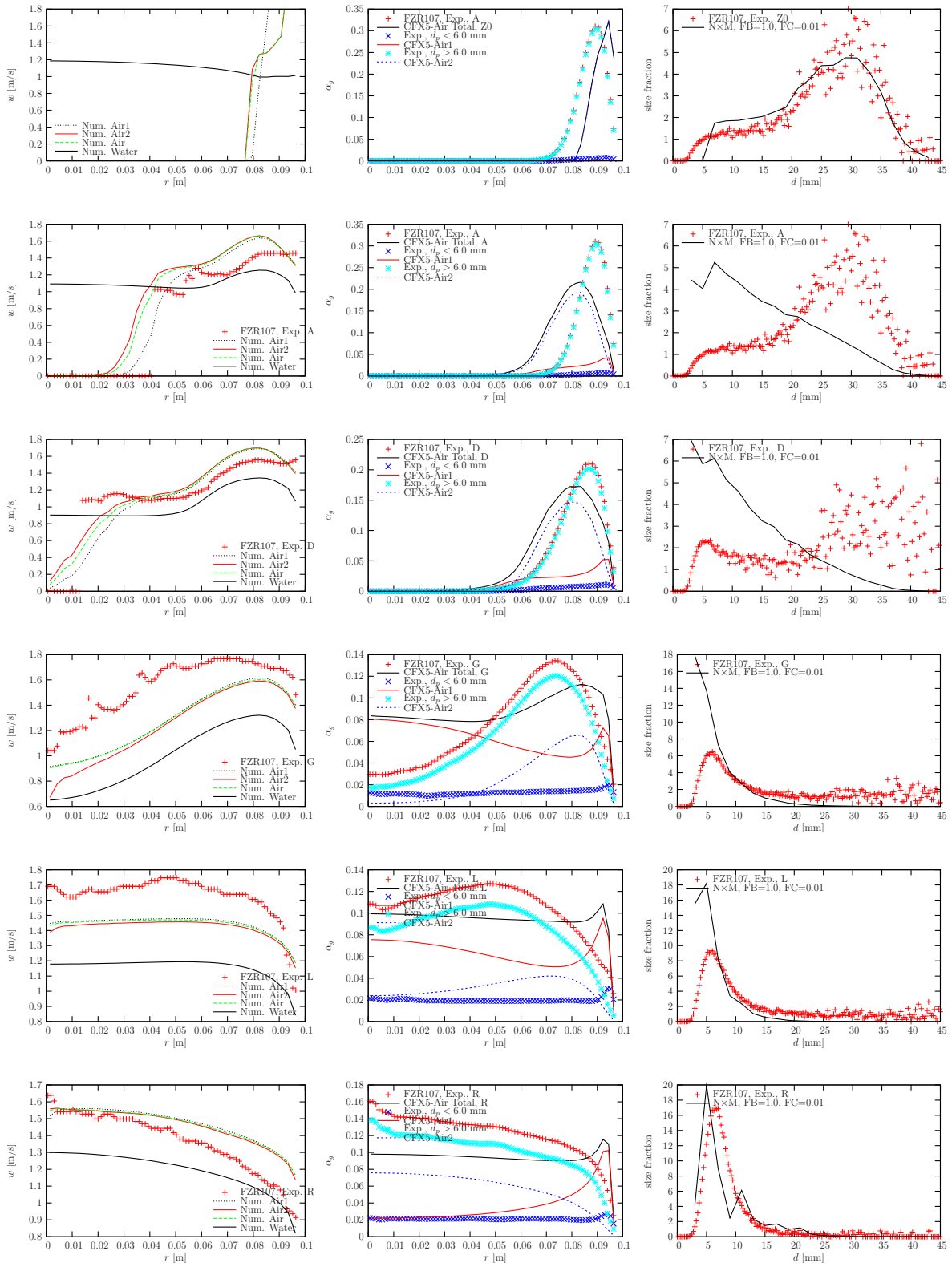

Fig. 5.1: Comparison of experimental and numerical results for the radial velocity and gas volume fraction profile and the average bubble size fraction distribution. Test case 107, with $FB = 1.0$ and $FC = 0.01$.

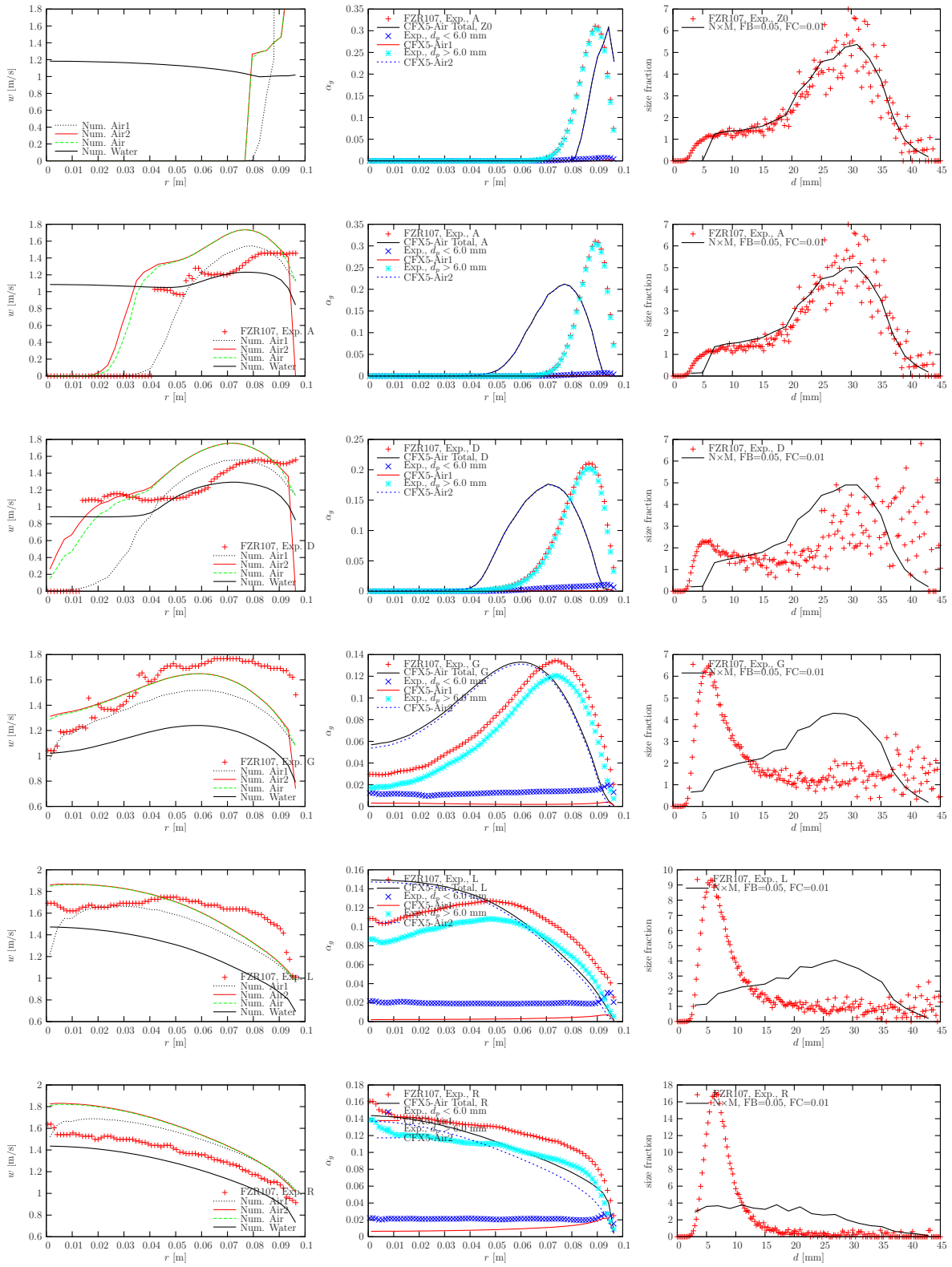

Fig. 5.2: Comparison of experimental and numerical results for the radial velocity and gas volume fraction profile and the average bubble size fraction distribution. Test case 107, with $FB = 0.05$ and $FC = 0.01$.

the measurement data, despite the deviations observed in the bubble size fraction distributions. This onfirms again that the $N \times M$ MUSIG model is capable of simulating inhomogeneous poly-dispersed flows so long as an accurate breakup and coalescence model will be available.

6 Summary

In this report we summarize our efforts in the development and validation of an efficient inhomogeneous Multiple Size Group model, which is called $N \times M$ MUSIG model in CFX10.0, in cooperation with ANSYS CFX. A novel multi-field multi-size group model was proposed for the simulation of inhomogeneous polydispersed flows (Krepper et al., 2003; Zwart et al., 2003). The model is based on the multi-fluid Eulerian approach and the population balance method. The dispersed phase can be divided into a small number of velocity groups, which are treated as phases with own velocity fields and interfacial interaction closures. Thereby the inhomogeneous motions of various velocity groups of the dispersed phase can be taken into account. The population balance method is applied to model the breakup and coalescence process. The velocity groups can further be devided into a number of sub-size classes. The population balance equation is applied to describe the inter-size class mass transfer. We also carried out a preliminary investigation using the $N \times 1$ variant, namely N velocity groups and each has one size groups (Shi et al., 2004a,b). Based on our continuous efforts, the $N \times M$ MUSIG model has beeen implemented in the commercial code ANSYS CFX10.0.

Detailed model validation were carried out by numerical and experimental investigations of air-water bubbly flows in a vertical pipe on the FZR TOPFLOW facility. The bubbles were divided into two velocity groups according to the direction of the lift force and into 21 size groups. The Prince and Blanch model (Prince and Blanch, 1990) was appied for describing the coalescence process and Luo and Svendsen model (Luo and Svendsen, 1996) for the breakup process. The model performance was examined in flows both with a low gas concentration (TOPFLOW-074) and with a high gas concentration (TOPFLOW-107), according to the radial distribution of the gas velocity at various levels and the volume fraction and the average bubble size fraction distribution over the corss sections of the pipe. Remarkably good agreements between the prediction and measurement were obtained in the low concentration case (TOPFLOW-074) by using a model cofficient $FC = 0.01$ for the Prince and Blanch model and $FB = 1.0$ for the Luo and Svendsen model. In the high concentration case (TOPFLOW-107), the $N \times M$ MUSIG model was also capable of predicting the development of the velocity and volume fraction profiles along the pipe and the correct bubble size fraction distribution in the fully developed flow at the upper levels. Nevertheless, the evolution of the bubble size fraction distribution along the pipe observed in the experiment could not be correctly predicted using the coalescence and breakup model. In addition, the lateral spreading of the gas phase close to the injection plane was too fast in both cases. The results suggest a need in detailed investigation and improvement of the bubble breakup and coalescence models by using a larger database of detailed and reliable experimental data at different flow conditions. The results also indicate that the effects of the high gas concentration of the interfacial force models have to be taken into account.

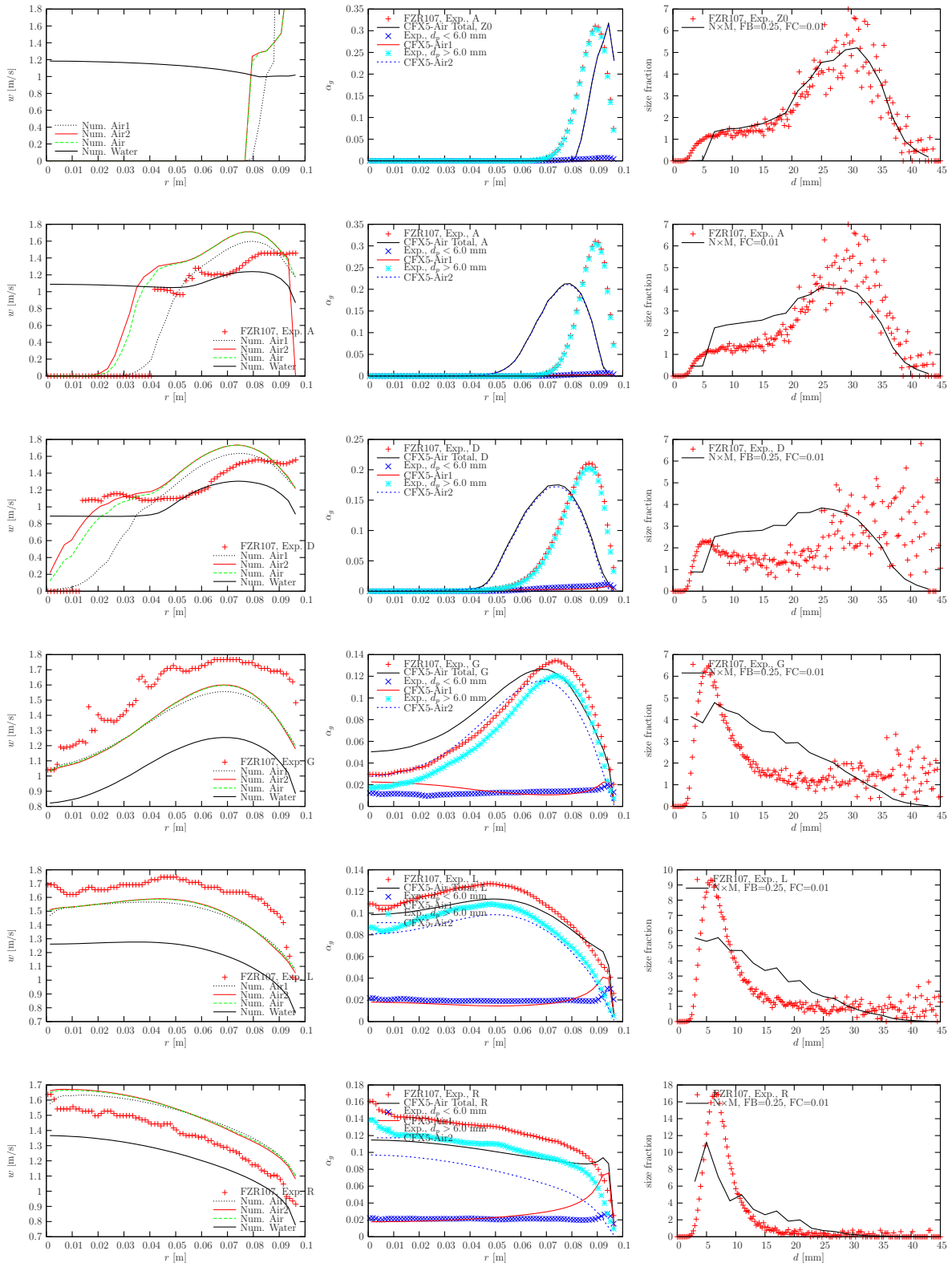

Fig. 5.3: Comparison of experimental and numerical results for the radial velocity and gas volume fraction profile and the average bubble size fraction distribution. Test case 107, with $FB = 0.25$ and $FC = 0.01$.

Acknowledgments

The model concept was proposed based on the extensive investigations carried out at Forschungszentrum Rossendorf (FZR). The development and validation was performed through close collaboration between FZR and ANSYS Germany. Thank Philip Zwart at ANSYS Canada Ltd. and Alan Burns at ANSYS Europe for valuable discussions and for providing useful documents.

References

Lo., S. (1996). Application of population balance to cfd modelling of bubbly flow via the MUSIG model. Technical Report AEAT-1096, AEA Technology plc.

Tomiyama, A. (1998). Struggle with computational bubble dynamics. In Third International Conference on Multiphase Flow, ICMF 98, Lyon, France.

Tomiyama, A., A. Sou, I. Zun, N. Kanami, and T. Sakaguchi (1995). Effect of Etvs number and dimensionless liquid volumetric flux on lateral montion of a bubble in a laminar duct flow. In A. Serizawa, T. Fukano, and J. Bataille, editors, Advances in Multiphase Flow, pages 3–15. Elsevier Science.

Lucas, D., E. Krepper, and H.-M. Prasser (2003). Evolution of flow patterns, gas fraction profiles and bubble size distributions in gas-liquid flows in vertical tubes. Transactions of the Institute of Fluid-Flow Machinery, 112:37–46.

Prasser, H.-M., E. Krepper, and D. Lucas (2003). Evolution of the two-phase flow in a vertical tube - decomposition of gas fraction profiles according to bubble size classes using wire-mesh sensors. Int. J. of Thermal Sciences, 41:17–28, 2002.

Krepper, E. and H.-M. Prasser (2000). Measurements and CFX simulations of a bubbly flow in a vertical pipe. In AMIFESF Workshop, Computing methods for two-phase flow, pages 1–8. 2000.

Shi, J.-M., E. Krepper, D. Lucas, and U. Rohde (2003). Some concepts for improving the MUSIG model. Technical report, Institute of Safety Research, Forschungszentrum Rossendorf, March, 2003. submitted to CFX Germany.

Zwart, P., A. Burns, and C. Montavon (2003). Multiple size group models. Technical report, AEA Technology plc, Novermber, 2003. CFX-5.7.

Shi, J.-M., T. Frank, H.-M. Prasser, and U. Rohde (2004a). N $\times$ 1 MUSIG model – implementation and application to gas-liquid flows in a vertical pipe. In ANSYS CFX & ICEM CFD Conference 2004, Dresden, 10.-12. November, 2004.

Shi, J.-M., P.J. Zwart, T. Frank, U. Rohde, and H.-M. Prasser (2004b). Development of a multiple velocity multiple size group model for poly-dispersed multiphase flows. In Annual Report of Institute of Safety Research. Forschungszentrum Rossendorf, Germany, 2004.

Prasser, H.-M., M. Beyer, A. Bttger, H. Carl, D. Lucas, A. Schaffrath, P. Schütz, Weiss F.-P., and J. Zschau (2003). Influence of the pipe diameter on the structure of the gas-liquid interface in a vertical two-phase pipe flow. In NURETH-10, Seoul, Korea, October 5-9, 2003. paper A00308.

Sato, Y. and K. Sekoguchi (1975). Liquid velocity distribution in two phase bubble flow. Int. J. Multiphase Flow, 2:79, 1975.

Sato, Y., M. Sadatomi, and K. Sekoguchi (1981). Momentum and heat transfer in two-phase bubbly flow. Int J Multiphase Flow, 7:167–178, 1981.

Grace, J. R. and M. E. Weber (1982). Handbook of Multiphase Systems, chapter Hydrodynamics of drops and bubbles. Hemisphere, 1982.

Burns, A., Th. Frank, I. Hamill, and J.-M. Shi (2004). The Favré averaged drag model for e turbulence dispersion in Eulerian multiphase flow. In ICMF 2004, 5th Int. Conf. Multiphase Flow, Yokohama, Japan, 2004.

Shi, J.-M., A. Burns, and H.-M. Prasser (2005). Turbulent dispersion of bubbles in polydispersed gas-liquid flows in a vertical pipe. pages 1–8, Beijing, China, May 15–20, 2005. Paper No. 50809.

Shi, J.-M., Th. Frank, E. Krepper, D. Lucas, U. Rohde, and H.-M. Prasser (2004c). Implementation and validation of non-drag interfacial forces in CFX-5.6. In ICMF 2004, 5th Int. Conf. Multiphase Flow, Yokohama, Japan, May 30-June 4, 2004.

Prince, M.J. and H.W. Blanch (1990). Bubble coalesce and break-up in air-sparged bubble columns. AIChE J., 36:1485–1499, 1990.

Luo, H. and F. Svendsen (1996). Theoretical model for drop and bubble break-up in turbulent dispersions. AIChE J., 42:1225–1233, 1996.

List of Figures

List of Tables